Frequency-Domain Differential Interference Cancellation for Full-Duplex OFDM ISAC Systems

Baiyu Duan, *Student Member, IEEE*, Cong Chen, Wensheng Pan, Ying Shen, Ying Liu, *Senior Member, IEEE*, and Shihai Shao, *Member, IEEE*

***Abstract*—The application of in-band full-duplex (IBFD) integrated sensing and communications (ISAC) systems for higher spectral efficiency and lower sensing latency has received increasing interest in recent years. In the IBFD mode, however, the transmitted signal causes severe interference at the receiver. This paper proposes a novel low-complexity frequency-domain differential interference cancellation (F-DIC) scheme for IBFD orthogonal frequency-division multiplexing (OFDM) ISAC systems. Without the need for channel state information (CSI), the proposed F-DIC method cancels the static interference and extracts the moving target echo signals by leveraging the invariant property of the interference. After the residual interference evaluation of the proposed method, the interference cancellation ratio of the F-DIC scheme is analyzed, and a closed-form formula of the target detection probability under the Neyman-Pearson (NP) criterion for OFDM ISAC systems based on the proposed scheme is also derived. Simulation results show that the proposed F-DIC method with promising low computational complexity performs similarly compared with the conventional frequency-domain interference cancellation method based on least squares (LS) and recursive least squares (RLS) algorithms.**

***Index Terms*—Digital cancellation, integrated sensing and communications (ISAC), in-band full-duplex (IBFD), orthogonal frequency-division multiplexing (OFDM).**

I. Introduction

DUE to a large number of emerging applications, such as the industrial Internet-of-Things (IIOT) and the vehicle-to-everything (V2X), demanding high-quality wireless connectivity as well as highly promising sensing capability, the integrated sensing and communications (ISAC) technology based on orthogonal frequency-division multiplexing (OFDM) waveforms is becoming a research hotpot for the next generation wireless networks (such as beyond 5G (B5G) and 6G) [1], [2], [3]. In order to achieve high spectral efficiency and low-latency sensing capabilities, OFDM ISAC systems with the in-band full-duplex (IBFD) mode have received widespread attention [1], [2], [4], [5], [6], [7], [8], which transmit communication signals and receive reflected signals from the environment simultaneously.

In the IBFD mode, however, severe interference will be introduced into the receiver. There are three types of signals received by the receiver at the same time and frequency caused by the transmitted signal in the OFDM ISAC system: the direct self-interference (SI) from the transmitter; the echo interference (also known as the multipath interference) reflected by objects in the environment; the target echo signals reflected by the desired targets [9]. The direct SI can obscure the desired targets in close range and at low speed in the range-velocity image of the OFDM radar and may even completely cover them due to its high power, which leads to severe performance degradation in the sensing system [5]. On the other hand, although the multipath interference has lower power compared with the direct SI, for it undergoes a long reflection path and the reflectors absorb part of its energy, it may still mask the targets around the reflectors in the range-velocity image and lead to a misjudgment of the target. Therefore, it is necessary to perform interference cancellation at the receiver of the ISAC system to enhance its sensing capability.

It is worth noting that the full-duplex manner in this paper means the base station (BS) receiver operates simultaneously while transmitting, i.e., the signal sent by the BS to realize simultaneous downlink communication and radar sensing while the receiver of the BS remains active for the reception of the echo [10], [11], [12], [13]. Additionally, rather than the IBFD communication system where all the three types of aforementioned signals need to be canceled at the receiver [14], the ISAC system aims at canceling the direct SI and the multipath interference (collectively called SI below) while retaining the target echoes.

The ISAC system can adopt some interference cancellation methods similar to those in the IBFD communication system. For instance, a high-isolation antenna can provide a TX-RX passive isolation of above 65 dB [15]. Another alternative of space domain interference cancellation is using array beamforming for active space domain isolation, by which a space isolation of at least about 40 dB between the transceiver array elements can be achieved [16], [17], [18]. To further cancel the SI, the IBFD system usually performs the radio frequency (RF) cancellation after the space domain isolation, utilizing the RF taps for active interference cancellation in the RF domain [5], [14], [15]. However, residual SI still exists after the first two interference cancellation stages, whose primary purpose is to

Manuscript received 10 November 2023; revised 20 January 2024; accepted 1 February 2024. Date of publication 6 February 2024; date of current version 20 June 2024. This work was supported by the National Natural Science Foundation of China under Grant U19B2014, Grant 62071094, and Grant 61901396. The review of this article was coordinated by Dr. Nghi H. Tran. *(Corresponding authors: Shihai Shao; Cong Chen.)*

The authors are with the National Key Laboratory of Wireless Communications, University of Electronic Science and Technology of China, Chengdu 611731, China, and also with the Laboratory of Electromagnetic Space Cognition and Intelligent Control, University of Electronic Science and Technology of China, Beijing 100089, China (e-mail: dby@std.uestc.edu.cn; chencong158@139.com; panwens@uestc.edu.cn; shenying@uestc.edu.cn; yliu85@uestc.edu.cn; ssh@uestc.edu.cn).

Digital Object Identifier 10.1109/TVT.2024.3362400

prevent the receiver saturation and maintain a sufficient dynamic range for the receiver receiving the desired signal [5], [6], [14]. In order to fully suppress the SI down to the noise floor, additional interference cancellers in the digital domain are still required at the receiver [5], [14], [15]. There are generally three kinds of digital interference cancellers, i.e., time-domain (TD) interference canceller [5], [9], [14], [19], frequency-domain (FD) interference canceller [20], [21], [22], and spatial-domain (SD) interference canceller [10], [11], [12], [13], [14], [16], [17].

Conventional TD methods are based on the least squares (LS) algorithm, which is also called extensive cancellation algorithm (ECA) in passive radar systems to suppress the static SI by using the uncorrelation between it and the Doppler-shifted echoes [9], [23]. However, the computational complexity of the LS method is usually very high under the multipath interference scenario. Therefore, the adaptive filter algorithms, i.e., recursive least squares (RLS) method and normalized least mean squares (NLMS) method, are widely used for lower complexity [5], [9], [19]. A TD nonlinear digital canceller is proposed in [5] to cancel the residual interference after the RF canceller. In order to avoid suppressing the echoes from the true targets, the canceller has a maximum cancellation delay or range, which is decided by the order of the transversal filter. Within this range, signals from the transmitter, including the direct SI and the close-range reflection echoes, can be effectively eliminated. Nevertheless, the TD methods cannot cancel the multipath interference outside the maximum cancellation range.

The conventional FD methods for canceling the SI in the frequency domain are also based on the LS algorithm [14], [20], [21]. Similar to TD methods, RLS and NLMS algorithms are applied in the frequency domain [21]. FD methods usually demonstrate lower computational complexity compared to TD methods with the merit of efficient operations such as discrete Fourier transform (DFT) or fast Fourier transform (FFT) processing. These operations are computationally less demanding than the convolution used in TD methods [20]. Additionally, in the context of the OFDM ISAC system, FD interference cancellation methods can achieve even lower computational complexity by multiplexing the existing FFT module in the OFDM receiver for signal demodulation. Furthermore, regardless of lower complexity, FD methods have almost the same interference cancellation performance compared with the TD methods [20], [21], [22].

To realize the SI cancellation while communicating with the users and sensing the desired targets, the SD interference cancellers in the full-duplex ISAC system have to take the constraint of sensing performance into account [10], [11], [12], [13]. This is different from the SD interference cancellers in the IBFD communication system [16], [17], of which the purpose is only to minimize the power of the SI. Studies in [10], [11] aim to optimize the beampattern for downlink communication signal and sensing performance while canceling the multiuser interference and the SI, respectively. In addition, authors in [12], [13] investigate the joint optimization for general ISAC involving IBFD communication and sensing while SI cancellation is also considered. Although SD cancellers have many advantages, some deficiencies of the SD methods exist in particular scenarios in spite of the common need for prior knowledge of the SI channel state information (CSI) matrix. Firstly, the interference cancellation performance of the SD methods will be reduced if targets and the direct SI or strong echo interference reflectors appear in the same beam. Under this circumstance, cascading with other TD/FD digital cancellers is a feasible way for SD cancellers to improve their performance. Moreover, for some miniaturized and energy-sensitive devices in ISAC systems, e.g., the micro-robot in some industrial networks [2] and the miniature unmanned aerial vehicle (UAV) in UAV networks [3], deploying multiple antennas on those devices incurs high implementation costs and power consumption, which may not be acceptable.

Considering that the direct SI has no Doppler shift, and the majority of the echo interference, i.e., the multipath interference, is reflected by stationary objects with no or sufficiently small Doppler shift [9], this paper proposes a low-complexity frequency-domain differential interference cancellation (F-DIC) method for IBFD OFDM ISAC systems. By leveraging the distinct Doppler properties of the target signals and the interference signals, and based on the low-complexity differential scheme [24], [25], [26], this method can effectively cancel the static SI while extracting the moving target echo signals. The F-DIC scheme takes advantage of the invariant property of the interference and performs differential operation on the received signal in the frequency domain, allowing interference cancellation without the need for the CSI. Note that the F-DIC is a digital FD cancellation method, and as mentioned above, to prevent the receiver from saturation, adequate space domain isolation and RF domain interference cancellation (if necessary) are required before performing the interference cancellation in the OFDM ISAC systems.

The contributions of this paper are summarized as follows:

- A novel low-complexity FD interference cancellation method is proposed for full-duplex OFDM ISAC systems, which can cancel the static SI while extracting the moving target echoes without the need for the CSI.[1]
- The influence of residual interference caused by the proposed F-DIC method is evaluated.
- The interference cancellation performance of the proposed F-DIC scheme is analytically analyzed in terms of the interference cancellation ratio (ICR).
- A closed-form expression of detection probability based on the Neyman-Pearson (NP) criterion for the proposed scheme used in the OFDM radar is derived to evaluate the influence of the proposed F-DIC method on the target detection performance.
- Comparisons between the proposed F-DIC method and the conventional TD/FD interference cancellation methods based on LS, RLS, and NLMS algorithms are given. The proposed method has promising low complexity, and no additional complex multiplications are required in the proposed F-DIC method by multiplexing the operations

[1] Note that the proposed method does not work for stationary targets. However, it can cancel all the signals with zero Doppler shift for moving target echo extraction, which is the main purpose of the proposed method.

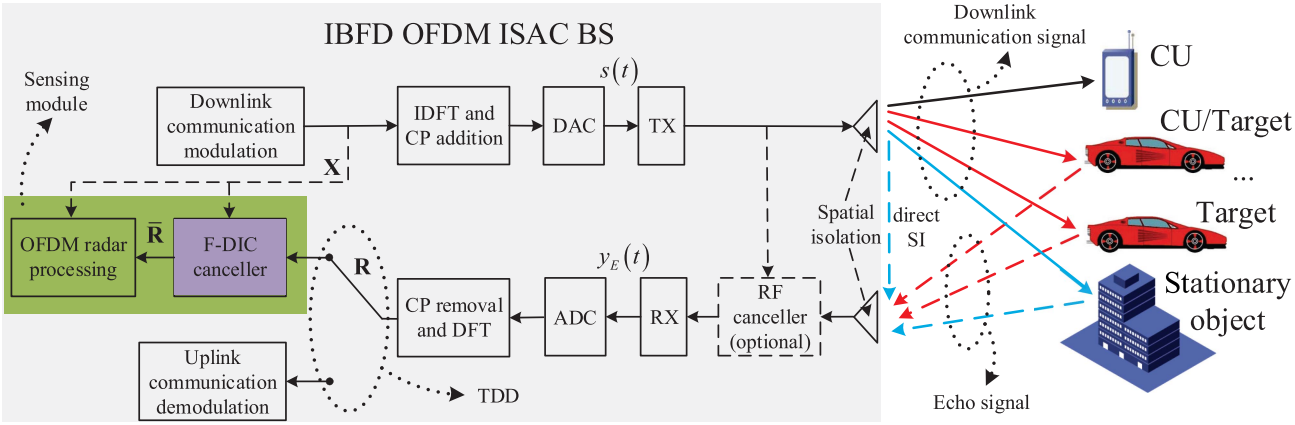

Fig. 1. Roadside scenario and system diagram of the OFDM ISAC system, where the solid lines represent the downlink signal and the dashed lines represent the received signal at the BS. Specifically, the blue dashed lines denote the static SI, while the red dashed lines are the moving target echoes. Note that the sensing and the communication function at the BS receiver is realized by the TDD mode.

of OFDM radar processing. Moreover, it achieves similar performance to the conventional FD LS/RLS interference cancellation methods.

The rest of the paper is organized as follows. The next section describes the system model of the IBFD OFDM ISAC system. In Section III, the property of the received signals is analyzed, and then, a novel low-complexity F-DIC scheme is proposed by leveraging the invariant property of the interference. Next, the evaluation of the proposed F-DIC method is provided in Section IV. In Section V, some numerical and simulation results are presented and discussed. Finally, Section VI concludes the whole paper.

Notations: In this paper, the set of complex values and positive integers are written as $\mathbb{C}$ and $\mathbb{Z}_{++}$, respectively, while boldface lower-case and boldface upper-case letters represent vectors and matrices, respectively. $X_{n,m}$ and $(\mathbf{X})_{n,m}$ are both denoted as the (n,m)-th entry of a matrix $\mathbf{X}$, and $\mathrm{diag}(\cdot)$ is a diagonal matrix. The transpose and the Hermitian transpose are denoted by $(\cdot)^T$ and $(\cdot)^H$, and $(\cdot)^*$ is the complex conjugate. $\odot$ represents the Hadamard product, and $|\cdot|$ is denoted as the absolute value. $\mathrm{E}[\cdot]$ is used for the expectation operation, while $\lfloor\cdot\rfloor$ is the floor function. In addition, $x \to a$ is defined as the relationship that x approaches a, while $lim_{x\to a} f(x)$ is the limit of the function $f(x)$ as x approaches a.

II. System Model

Consider a typical roadside ISAC BS scenario shown in Fig. 1. The BS transmits conventional OFDM waveforms to communicate with the users [27], e.g., autonomous vehicles and pedestrians, while sensing the moving targets using the echo signal of the OFDM waveforms at the same time. It is worth emphasizing that the moving targets may or may not be the communication user (CU), and the transmitted data can be known to the BS sensing receiver. This paper aims at extracting the moving target echo signals (red dashed lines in Fig. 1) while canceling the static SI (blue dashed lines in Fig. 1) at the BS receiver. As mentioned above, the IBFD manner in this paper means that the BS processes the sensing echo simultaneously while transmitting downlink communication waveforms. Therefore, the sensing and the communication function for uplink communication demodulation at the BS receiver operates in time division duplex (TDD) mode.

The complex baseband transmitted OFDM signal is written as [28]

$$s(t)=\frac{1}{\sqrt{N_{\mathrm{c}}}}\sum_{m=0}^{N_{\mathrm{s}}-1}\sum_{n=0}^{N_{\mathrm{c}}-1}X_{n,m}e^{j2\pi f_n(t-mT_{\mathrm{s}})}\mathrm{rect}\left(\frac{t-mT_{\mathrm{s}}+T_{\mathrm{cp}}}{T_{\mathrm{s}}}\right), \tag{1}$$

where $n=0,\ldots,N_{\mathrm{c}}-1$ and $m=0,\ldots,N_{\mathrm{s}}-1$ are the subcarrier index and the symbol index, respectively, while N_{c} and N_{s} represent the number of OFDM subcarriers and symbols, respectively. $X_{n,m}$ is the m-th normalized data symbol at the n-th subcarrier and there is $\mathrm{E}[|X_{n,m}|^2]=1$. Additionally, $f_n=n\Delta f$ denotes the n-th subcarrier frequency with a Δf subcarrier spacing. Furthermore, $T_{\mathrm{s}}=T_{\mathrm{e}}+T_{\mathrm{cp}}$ is defined as the overall OFDM symbol duration, with T_{e} and T_{cp} being the duration of the data symbol and the cyclic prefix (CP), respectively. And $\mathrm{rect}(t/T_{\mathrm{s}})$ denotes a rectangular function whose value is 1 for $t\in[0,\ T_{\mathrm{s}}]$ and 0 otherwise.

First of all, the following standard assumptions are made: (*i*) the targets are regarded as point targets for the OFDM radar, (*ii*) different targets are located in different range bins and velocity bins, which means the targets do not coincide, leading to the independence of the target echo signals, and (*iii*) the time-bandwidth product is considered to be low enough so that the wideband effect of the reflected echo signals is able to be ignored [4], [28]. As depicted in Fig. 1, the propagation paths from the BS transmitter to the BS receiver include the reflected paths (containing those for both the moving targets and the stationary objects) and the direct SI path. Assuming that the number of propagation paths is L, then the l-th propagation path can be characterized by the complex channel coefficient α_l, the time delay τ_l and the Doppler shift $(f_{\mathrm{D}})_l$. The noise-free TD

baseband received signal at the BS receiver can be expressed as

$$y_{\mathrm{E}}(t)=\sum_{l=0}^{L-1}\alpha_l s\left(t-\tau_l\right)e^{j2\pi(f_{\mathrm{D}})_l t}=\frac{1}{\sqrt{N_{\mathrm{c}}}}\sum_{l=0}^{L-1}\alpha_l e^{j2\pi(f_{\mathrm{D}})_l t}\times\sum_{m=0}^{N_{\mathrm{s}}-1}\sum_{n=0}^{N_{\mathrm{c}}-1}X_{n,m}e^{j2\pi f_n(t-mT_{\mathrm{s}}-\tau_l)}\mathrm{rect}\left(\frac{t-mT_{\mathrm{s}}+T_{\mathrm{cp}}-\tau_l}{T_{\mathrm{s}}}\right). \tag{2}$$

After sampling (2) at $t=mT_{\mathrm{s}}+kT_{\mathrm{e}}/N_{\mathrm{c}},\ k=0,\ldots,N_{\mathrm{c}}-1$ and removing the CP (assuming that the maximum propagation delay is smaller than T_{cp}), the discrete TD received signal is

$$y_{\mathrm{E}}(k,m)=\sum_{l=0}^{L-1}\frac{\alpha_l}{\sqrt{N_{\mathrm{c}}}}e^{j2\pi(f_{\mathrm{D}})_l\frac{k}{N_{\mathrm{c}}}T_{\mathrm{e}}}e^{j2\pi(f_{\mathrm{D}})_l mT_{\mathrm{s}}}\times\sum_{n=0}^{N_{\mathrm{c}}-1}X_{n,m}e^{-j2\pi f_n\tau_l}e^{j2\pi n\frac{k}{N_{\mathrm{c}}}}. \tag{3}$$

For the sake of convenience, the time delay vector, the Doppler phase vector, and the intercarrier interference (ICI) phase rotation matrix are respectively defined as

$$\mathbf{v}_{\tau_l}=\left[1,T_l,\ldots,(T_l)^{N_{\mathrm{c}}-1}\right]^T, \tag{4}$$

$$\mathbf{v}_{f_l}=\left[1,F_l,\ldots,(F_l)^{N_{\mathrm{s}}-1}\right]^T, \tag{5}$$

$$\mathbf{D}_{(f_{\mathrm{D}})_l}=\mathrm{diag}\left(1,D_l,\ldots,(D_l)^{N_{\mathrm{c}}-1}\right), \tag{6}$$

where $T_l=e^{-j2\pi\Delta f\tau_l}$, $F_l=e^{j2\pi(f_{\mathrm{D}})_l T_{\mathrm{s}}}$ and $D_l=e^{j2\pi(f_{\mathrm{D}})_l T_{\mathrm{e}}/N_{\mathrm{c}}}$. Thus, (3) can be rewritten as [7]

$$\mathbf{Y}_{\mathrm{E}}=\sum_{l=0}^{L-1}\alpha_l\mathbf{D}_{(f_{\mathrm{D}})_l}\mathbf{F}_{N_{\mathrm{c}}}^H\left[\mathbf{X}\odot\mathbf{v}_{\tau_l}\mathbf{v}_{f_l}^H\right]\in\mathbb{C}^{N_{\mathrm{c}}\times N_{\mathrm{s}}}, \tag{7}$$

in which $\mathbf{F}_N\in\mathbb{C}^{N\times N}$ refers to the unitary DFT matrix with $(\mathbf{F}_N)_{k,n}=\frac{1}{\sqrt{N}}e^{-j2\pi nk/N}$, and $\mathbf{X}\in\mathbb{C}^{N_{\mathrm{c}}\times N_{\mathrm{s}}}$ is the data symbol matrix with $(\mathbf{X})_{n,m}=X_{n,m}$. After performing an N-point DFT operation to (7), the FD received signal is given in matrix form by

$$\mathbf{R}_{\mathrm{E}}=\sum_{l=0}^{L-1}\alpha_l\mathbf{F}_{N_{\mathrm{c}}}\mathbf{D}_{(f_{\mathrm{D}})_l}\mathbf{F}_{N_{\mathrm{c}}}^H\left[\mathbf{X}\odot\mathbf{v}_{\tau_l}\mathbf{v}_{f_l}^H\right]\in\mathbb{C}^{N_{\mathrm{c}}\times N_{\mathrm{s}}}. \tag{8}$$

III. Frequency-Domain Differential Interference Cancellation

In this section, the expression of the received OFDM subcarrier with ICI is derived and analyzed first to figure out the influence of the Doppler shift on the received OFDM signal. Then, a novel low-complexity F-DIC method by leveraging the invariant property of the interference channel is proposed.

A. Doppler Shift Influence

Firstly, consider the special case where there is only one propagation path in the channel, and the subscript l is temporarily dropped for simplicity. The received signal at the n-th subcarrier of the m-th OFDM symbol derived from (8) can be expressed as (see Appendix A for the proof)

$$(\mathbf{R}_{\mathrm{sig}})_{n,m}=\alpha\zeta_n T^n F^m X_{n,m}+\sum_{k=0,\ k\neq n}^{N_{\mathrm{c}}-1}\alpha\zeta_k X_{k,m}T^k F^m, \tag{9}$$

where

$$\zeta_k=\frac{1-D^{N_{\mathrm{c}}}}{N_{\mathrm{c}}\left(1-DW^{-k+n}\right)}=\frac{1-e^{j2\pi f_{\mathrm{D}}T_{\mathrm{e}}}}{N_{\mathrm{c}}\left(1-e^{j2\pi(f_{\mathrm{D}}T_{\mathrm{e}}+k-n)/N_{\mathrm{c}}}\right)}, \tag{10}$$

and

$$\zeta\triangleq\zeta_n=\frac{1-D^{N_{\mathrm{c}}}}{N_{\mathrm{c}}\left(1-D\right)}=\frac{1-e^{j2\pi f_{\mathrm{D}}T_{\mathrm{e}}}}{N_{\mathrm{c}}\left(1-e^{j2\pi f_{\mathrm{D}}T_{\mathrm{e}}/N_{\mathrm{c}}}\right)}, \tag{11}$$

with $W=e^{-j2\pi/N_{\mathrm{c}}}$. Then the channel matrix of the single path can be obtained by $\mathbf{H}_{\mathrm{sig}}=\mathbf{R}_{\mathrm{sig}}./\mathbf{X}$, where $./$ denotes the element-wise division, which is

$$(\mathbf{H}_{\mathrm{sig}})_{n,m}=\alpha\zeta T^n F^m+\sum_{k=0,\ k\neq n}^{N_{\mathrm{c}}-1}\alpha\zeta_k\frac{X_{k,m}}{X_{n,m}}T^k F^m. \tag{12}$$

For the coefficient ζ, when $f_{\mathrm{D}}\to 0$, both the numerator and the denominator of ζ tend to 0. Hence, the exponential term in ζ can be expanded by Maclaurin's series, and it yields $\zeta\approx 1$ by taking the first two terms of the series. For the other coefficients $\zeta_k,\ k\neq n$, it can be observed that $-1<(f_{\mathrm{D}}T_{\mathrm{e}}+k-n)/Nc<1$ if $f_{\mathrm{D}}\to 0$. When $e^{j2\pi(f_{\mathrm{D}}T_{\mathrm{e}}+k-n)/N_{\mathrm{c}}}\approx 1$, i.e., $|f_{\mathrm{D}}T_{\mathrm{e}}+k-n|/N_{\mathrm{c}}\to 0$ or 1, the exponential term of ζ_k can also be expanded by the Maclaurin's series, and it yields $\zeta_k\approx\frac{1}{1+(k-n)/f_{\mathrm{D}}T_{\mathrm{e}}}(k\neq n)\approx 0$. When $e^{j2\pi(f_{\mathrm{D}}T_{\mathrm{e}}+k-n)/N_{\mathrm{c}}}\neq 1$, the numerator of ζ_k tends to 0 if $f_{\mathrm{D}}\to 0$. Considering that the value of N_{c} in the denominator is relatively large (usually from hundreds to thousands), the value of ζ_k still tends to 0, i.e., $\zeta_k\approx 0$. To sum up, there are $\zeta\approx 1$ and $\zeta_k\approx 0$ when $f_{\mathrm{D}}\to 0$.

From the above discussion, it can be seen that the ICI introduces a complex coefficient ζ as well as additive interference to the given subcarrier channel. It is also shown that when $f_{\mathrm{D}}\to 0$, i.e., when the target velocity is relatively low, the complex coefficient $\zeta\approx 1$ and the additive interference is negligible. As a result, the channel matrix in (12) reduces to $(\mathbf{H}_{\mathrm{sig}})_{n,m}=\alpha T^n F^m$, when $f_{\mathrm{D}}=0$.

Next, consider the general case where there are L echo signals, including P moving target echo signals and Q static echo signals, i.e., $L=P+Q$. Then the channel matrix $\mathbf{H}$ can be divided into two parts, i.e., the moving channel matrix $\mathbf{H}^{\mathrm{M}}$ with Doppler shift and the static channel matrix $\mathbf{H}^{\mathrm{S}}$ without Doppler shift, where $\mathbf{H}=\mathbf{H}^{\mathrm{M}}+\mathbf{H}^{\mathrm{S}}$. According to (12), the elements of the channel matrix $\mathbf{H}$ in the case with multiple paths can be written as

$$H_{n,m}=\sum_{l=0}^{L-1}\alpha_l\left(F_l\right)^m\left[\zeta_l\left(T_l\right)^n+\sum_{k=0,\ k\neq n}^{N_{\mathrm{c}}-1}\zeta_k^l\frac{X_{k,m}}{X_{n,m}}\left(T_l\right)^k\right]=H_{n,m}^M+H_{n,m}^S, \tag{13}$$

where

$$H_{n,m}^{M}=\sum_{p=0}^{P-1}\alpha_p\left(F_p\right)^m\left[\zeta_p\left(T_p\right)^n+\sum_{k=0,\ k\neq n}^{N_c-1}\zeta_k^p\frac{X_{k,m}}{X_{n,m}}\left(T_p\right)^k\right], \tag{14}$$

$$H_{n,m}^{S}=\sum_{q=0}^{Q-1}\alpha_q\left(T_q\right)^n, \tag{15}$$

with $\zeta_l=\frac{1-(D_l)^{N_c}}{N_c(1-D_l)}$ and $\zeta_k^l=\frac{1-(D_l)^{N_c}}{N_c(1-D_lW^{-k+n})}$.

From (14) and (15), the relationship between the channels for two successive OFDM symbols at the same subcarrier can be derived for the moving channel and the static channel, respectively, i.e., $H_{n,m+1}^{M}=\kappa(\alpha_p,T_p,F_p,\zeta_p,\zeta_k^p,X_{n,m+1},X_{n,m})H_{n,m}^{M}$ (in which κ is a complex coefficient), and $H_{n,m+1}^{S}=H_{n,m}^{S}$. It can be seen that the static channels for two successive OFDM symbols at the same subcarrier are identical, while the moving channels for them are different due to the Doppler shift.

In addition, there may exist some slow movement of the static sources (e.g., branches of trees or water waves), leading to some spread in the frequency domain of the corresponding channel. Those channels can also be defined as the static channel by adding a small deviation value $\Delta_{n,m}$, where $\Delta_{n,m}=H_{n,m+1}^{S}-H_{n,m}^{S}$ represents the small gap between the static channels for two successive OFDM symbols at the same subcarrier. Based on the different characteristics of the moving and static channels mentioned above, the FD differential processing can be performed to cancel the static SI while extracting the moving target echo signals.

B. F-DIC Method

The FD differential processing of the proposed F-DIC method is performed along successive OFDM symbols at the same subcarrier. The received signal, including thermal noise at the n-th subcarrier of the m-th OFDM symbol in the frequency domain, can be expressed as

$$\begin{aligned}R_{n,m}&=H_{n,m}X_{n,m}+N_{n,m}=H_{n,m}^{M}X_{n,m}\\&\quad+H_{n,m}^{S}X_{n,m}+N_{n,m},\end{aligned} \tag{16}$$

where $N_{n,m}$ is the circular symmetric complex Gaussian (CSCG) noise with zero mean and a variance of N_0. Denoting the useful signal for sensing (i.e., the moving target echo signals) by $E_{n,m}=H_{n,m}^{M}X_{n,m}$, the differential signal sequence can be obtained as

$$\begin{aligned}T_{n,m}&=R_{n,m}-\frac{X_{n,m}}{X_{n,m+1}}R_{n,m+1}\\&=E_{n,m}+N_{n,m}-\frac{X_{n,m}}{X_{n,m+1}}\left(E_{n,m+1}+N_{n,m+1}\right)\\&\quad-X_{n,m}\Delta_{n,m},\ n=0,\ldots N_c-1,\ m=0,\ldots,N_s-2.\end{aligned} \tag{17}$$

Using the smoothing scheme proposed in [24], a new recursion formula is defined as

$$\begin{aligned}U_{n,0}&=T_{n,0}=E_{n,0}+N_{n,0}-\frac{X_{n,0}}{X_{n,1}}\left(E_{n,1}+N_{n,1}\right)-X_{n,0}\Delta_{n,0},\\U_{n,m}&=U_{n,m-1}+\frac{X_{n,0}}{X_{n,m}}T_{n,m}\\&=E_{n,0}+N_{n,0}-\frac{X_{n,0}}{X_{n,m+1}}\left(E_{n,m+1}+N_{n,m+1}\right)\\&\quad-X_{n,0}\sum_{k=0}^{m}\Delta_{n,m},\ m=1,\ldots,N_s-2.\end{aligned} \tag{18}$$

Then, the estimated value of $E_{n,0}+N_{n,0}$ is obtained as

$$\hat{E}_{n,0}=\frac{1}{N_s-1}\sum_{m=0}^{N_s-2}U_{n,m}=E_{n,0}+N_{n,0}+W_{n,0}, \tag{19}$$

where $W_{n,0}$ is the residual interference at the n-th subcarrier of the first OFDM symbol, which can be expressed as

$$\begin{aligned}W_{n,0}=&-\frac{1}{N_s-1}\sum_{m=0}^{N_s-2}\left[\frac{X_{n,0}}{X_{n,m+1}}\left(E_{n,m+1}+N_{n,m+1}\right)\right.\\&\left.+X_{n,0}\left(N_s-1-m\right)\Delta_{n,m}\right].\end{aligned} \tag{20}$$

Substituting (19) into (18), $U_{n,m-1}$ is rewritten as

$$U_{n,m-1}=\hat{E}_{n,0}-\frac{X_{n,0}}{X_{n,m}}\hat{E}_{n,m}. \tag{21}$$

Therefore, the estimated value of $E_{n,m}+N_{n,m}$ can be calculated as

$$\hat{E}_{n,m}=\frac{X_{n,m}}{X_{n,0}}\left(\hat{E}_{n,0}-U_{n,m-1}\right)=E_{n,m}+N_{n,m}+W_{n,m}, \tag{22}$$

where $W_{n,m}$ is the residual interference at the n-th subcarrier of the m-th OFDM symbol and can be represented as

$$W_{n,m}=X_{n,m}\left(\frac{W_{n,0}}{X_{n,0}}+\sum_{k=0}^{m-1}\Delta_{n,k}\right),m=1,\ldots,N_s-1. \tag{23}$$

According to (22), the output signal after F-DIC can be written as

$$\bar{R}_{n,m}=\hat{E}_{n,m}=H_{n,m}^{M}X_{n,m}+N_{n,m}+W_{n,m}. \tag{24}$$

Finally, the procedures of the proposed F-DIC method are summarized in Algorithm 1.

IV. Evaluation of the Proposed Method

In this section, the influence of residual interference after the proposed method is presented first. Then, the performance of the proposed F-DIC scheme is analyzed in terms of the ICR and the detection probability of the sensing system. Furthermore, the computational complexity of the F-DIC method and the conventional TD/FD methods is given to show the promising low complexity of the proposed method. The last subsection discusses the output signal comparison between the proposed

Algorithm 1: Frequency-domain Differential Interference Cancellation.

Input: Received signal $R_{n,m}$ in (16).
Output: Output signal $\bar{R}_{n,m}$ after F-DIC in (24).
for $n = 0$ to $N_{\rm c} - 1$ **do**
Step 1: Calculate the differential sequence $T_{n,m}$ in (17).
Step 2: Calculate the recursion sequence $U_{n,0} = T_{n,0}$ and $U_{n,m} = U_{n,m-1} + \frac{X_{n,0}}{X_{n,m}} T_{n,m}$ in (18).
Step 3: Calculate the estimated values in (19) and (22), which are $\hat{E}_{n,0} = \frac{1}{N_{\rm s}-1} \sum_{m=0}^{N_{\rm s}-2} U_{n,m}$ and $\hat{E}_{n,m} = \frac{X_{n,m}}{X_{n,0}} (\hat{E}_{n,0} - U_{n,m-1})$, and then output $\hat{E}_{n,m}$.
end for

F-DIC and conventional frequency-domain least squares (F-LS) methods.

As aforementioned, since the moving targets do not coincide and are independent, only one moving target echo signal is taken into account, while the other echo signals are assumed to be static, i.e., $P = 1$ and $\Delta_{n,m} = 0$. As a result, the subscript p in (14) can be dropped in the following expressions.

According to (14), (15), and (16), the input signal before F-DIC can be rewritten as

$$\begin{aligned} R_{n,m} &= (R_{\rm E})_{n,m} + N_{n,m} = \alpha\zeta T^n F^m X_{n,m} \\ &+ \sum_{k=0,\ k\neq n}^{N_{\rm c}-1} \alpha\zeta_k T^k F^m X_{k,m} + \sum_{q=0}^{Q-1} \alpha_q \left(T_{\rm q}\right)^n X_{n,m} + N_{n,m} \\ &= (T_{\rm E})_{n,m} + I_{n,m} + (T_{\rm SI})_{n,m} + N_{n,m}, \end{aligned} \tag{25}$$

in which the first term is the target echo signal, i.e., the useful signal. The second term represents the additive ICI term for the useful signal. In addition, the third term expresses the sum of the static SI, while the last term is the thermal noise following a zero-mean complex Gaussian distribution, i.e., $N_{n,m} \sim \mathcal{CN}(0, \sigma_N^2)$, in which σ_N^2 is the power of the thermal noise. Based on (14), (23), and (24), the output signal after F-DIC is

$$\begin{aligned} \bar{R}_{n,m} &= \alpha\zeta T^n F^m X_{n,m} + \sum_{k=0,\ k\neq n}^{N_{\rm c}-1} \alpha\zeta_k T^k F^m X_{k,m} \\ &- \frac{X_{n,m}}{N_{\rm s}-1} \sum_{s=1}^{N_{\rm s}-1} \left(\alpha\zeta T^n F^s + \sum_{k=0,\ k\neq n}^{N_{\rm c}-1} \alpha\zeta_k \frac{X_{k,s}}{X_{n,s}} T^k F^s \right) \\ &+ N_{n,m} - \frac{X_{n,m}}{N_{\rm s}-1} \sum_{s=1}^{N_{\rm s}-1} \frac{N_{n,s}}{X_{n,s}} \\ &= (T_{\rm E})_{n,m} + \bar{W}_{n,m} + \bar{I}_{n,m} + \bar{N}_{n,m}, \end{aligned} \tag{26}$$

where

$$\bar{W}_{n,m} = -\frac{X_{n,m}}{N_{\rm s}-1} \sum_{s=1}^{N_{\rm s}-1} \alpha\zeta T^n F^s, \tag{27}$$

$$\begin{aligned} \bar{I}_{n,m} &= I_{n,m} + I_{n,m}^W = \sum_{k=0,\ k\neq n}^{N_{\rm c}-1} \alpha\zeta_k T^k F^m X_{k,m} \\ &- \frac{X_{n,m}}{N_{\rm s}-1} \sum_{s=1}^{N_{\rm s}-1} \sum_{k=0,\ k\neq n}^{N_{\rm c}-1} \alpha\zeta_k \frac{X_{k,s}}{X_{n,s}} T^k F^s, \end{aligned} \tag{28}$$

$$\bar{N}_{n,m} = N_{n,m} - \frac{X_{n,m}}{N_{\rm s}-1} \sum_{s=1}^{N_{\rm s}-1} \frac{N_{n,s}}{X_{n,s}}. \tag{29}$$

$\bar{W}_{n,m}$ represents the residual interference on the useful signal after F-DIC, and $\bar{I}_{n,m}$ is the sum of the ICI and the differential residual ICI caused by the F-DIC scheme. Additionally, $\bar{N}_{n,m}$ is the sum of the noise and differential residual noise, which is also a zero-mean complex Gaussian variable with a variance of $\sigma_{\bar{N}}^2 = \frac{N_{\rm s}}{N_{\rm s}-1} \sigma_N^2$ due to the linear combination property.

A. Residual Interference Analysis

The residual interference $\bar{W}_{n,m}$ in (27) can be regarded as the average value of the useful signal for OFDM symbols indexed 1 to $N_{\rm s} - 1$ at the n-th subcarrier. Hence, $\bar{W}_{n,m}$ can influence the useful signal under certain conditions. When the target velocity is extremely low, i.e., when $f_{\rm D} \to 0$, $(T_{\rm E})_{n,m} + \bar{W}_{n,m} \to 0$. This indicates that the residual interference $\bar{W}_{n,m}$ distorts the useful signal when the target speed is low. Additionally, in the case of the target velocity being 0 m/s, no output of the useful signal is observed after applying F-DIC. This is a reasonable phenomenon since the F-DIC scheme is designed to suppress the signal without the Doppler shift. Nevertheless, when the target velocity deviates from 0 m/s, the value of $\bar{W}_{n,m}$ remains relatively small, especially when $N_{\rm s}$ is large.

According to (25) and (27), the average power at the single subcarrier of the useful signal and the residual interference can be calculated as $p_{\rm E} = |\alpha|^2 |\zeta|^2$ and $p_{\rm W} = E[|\bar{W}_{n,m}|^2] = \frac{|\alpha|^2 |\zeta|^2}{(N_{\rm s}-1)^2} |\sum_{s=1}^{N_{\rm s}-1} F^s|^2$, respectively. In order to analyze the relationship between the residual interference and useful signal, the residual interference power to useful signal power ratio (ISR) is defined as

$$\text{ISR} \triangleq \frac{p_{\rm W}}{p_{\rm E}} = \frac{1}{(N_{\rm s}-1)^2} \left| \sum_{s=1}^{N_{\rm s}-1} F^s \right|^2. \tag{30}$$

Lemma 4.1: The value of ISR is (0,1]. And ISR can be written as

$$\text{ISR} = \begin{cases} 1, & f_{\rm D} = 0, \\ \frac{1}{N_{\rm s}-1} F_{N_{\rm s}-1}\left(2\pi f_{\rm D} T_{\rm s}\right), & f_{\rm D} \neq 0, \end{cases} \tag{31}$$

where $F_N(x)$ is the Fejér kernel [29]. There is

$$F_N(x) = \frac{1}{N} \frac{\sin^2\left(Nx/2\right)}{\sin^2\left(x/2\right)},\ x \in \mathbb{R},\ N \in \mathbb{Z}_{++}. \tag{32}$$

Proof: The proof is presented in Appendix B. ■

Proposition 4.1: When the velocity of the target is not 0 m/s, and the number of OFDM symbols $N_{\rm s}$ is sufficiently large, ISR

approaches 0, i.e., $\lim_{N_s\to\infty}\mathrm{ISR}=0$ if $f_D\neq 0$. Moreover, if the value of $(N_s-1)f_DT_s$ is small, ISR is closed to 1.

Proof: Based on Lemma 4.1, when $f_D\neq 0$, ISR can be rewritten as

$$\begin{aligned}\mathrm{ISR}&=\left\{\frac{\pi f_DT_s}{\sin\left(\pi f_DT_s\right)}\frac{\sin\left[\pi\left(N_s-1\right)f_DT_s\right]}{\pi\left(N_s-1\right)f_DT_s}\right\}^2\\&=\frac{\pi^2\left(f_DT_s\right)^2}{\sin^2\left(\pi f_DT_s\right)}\left\{\mathrm{sinc}\left[\left(N_s-1\right)f_DT_s\right]\right\}^2,\end{aligned}\tag{33}$$

where $\mathrm{sinc}(x)$ denotes the sinc function [27]. Hence, when $N_s\to\infty$, there is

$$\lim_{N_s\to\infty}\mathrm{ISR}=\frac{\pi^2\left(f_DT_s\right)^2}{\sin^2\left(\pi f_DT_s\right)}\lim_{N_s\to\infty}\left\{\mathrm{sinc}\left[\left(N_s-1\right)f_DT_s\right]\right\}^2=0.\tag{34}$$

Similarly, because of the sinc function, it is obvious that ISR is closed to 1 when $(N_s-1)f_DT_s$ is small. ■

Proposition 4.1 indicates that the residual interference after F-DIC is very small when the number of OFDM symbols is sufficiently large, as long as the target speed is not zero. Besides, it proposes that the residual interference is comparable to the useful signal if $(N_s-1)f_DT_s$ is small. In fact, since $f_DT_s\ll 1$ is common in the real OFDM radar system (for T_s is usually microseconds), if N_s is small, e.g., $N_s=2,4,8$, the residual interference is very large and has serious influence on the useful signal.

Proposition 4.2: If the target velocity is 0 m/s, ISR has the maximal value of 1. Furthermore, when $f_DT_s\leq 0.5$, with the increase of the target velocity, ISR approaches 0. ■

Proof: If the target velocity is zero, it can be known from Lemma 4.1 that ISR $=1$, which is also the maximal value of ISR. It is easy to know that Fejér kernel $F_N(x)$ is a positive even function of period 2π with the maximal value at $x=2k\pi,\ k=0,\pm1,\pm2,\ldots$. Furthermore, the value of Fejér kernel converges from the maximal value to zero in the cycle period [29], specifically, at $x\in[2k\pi,(2k+1)\pi],\ k=0,\pm1,\pm2,\ldots$. Thus, based on the property of the Fejér kernel, ISR approaches 0 with the increase of f_D when $2\pi f_DT_s\leq\pi$, i.e., when $f_DT_s\leq 0.5$.

Note that $f_DT_s\leq 0.5$ is an extremely accessible condition in the real OFDM radar system, for its value is usually much less than 1. Proposition 4.2 means that the residual interference of the proposed method is not only related to N_s but also influenced by the target velocity v. The residual interference power p_W increases when the target velocity decreases to 0 m/s and reaches the maximal value p_E at zero target velocity.

The above analysis focuses on the relationship between the residual interference and the useful signal. However, thermal noise also plays a crucial role in the interference cancellation method. The residual interference has little effect on the receiver system if the power of it is smaller than that of the noise. In other words, the relative magnitude of the residual interference and noise is also important. The noise power to useful signal power ratio (NSR) is denoted as $\mathrm{NSR}\triangleq p_{\bar{N}}/p_E$, in which $p_{\bar{N}}=\sigma_{\bar{N}}^2$. Therefore, to evaluate the influence of residual interference after the proposed method, the thermal noise is added, and the residual interference plus noise power to useful signal power ratio (INSR)

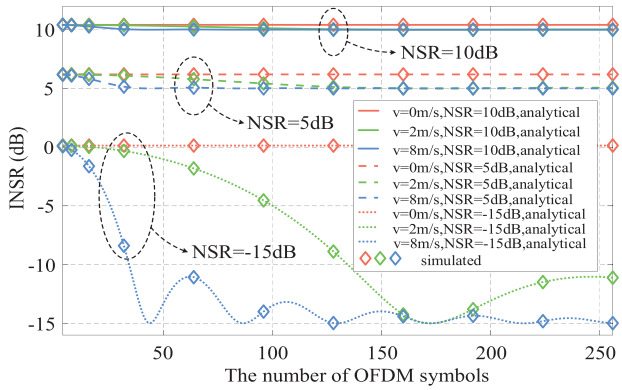

Fig. 2. INSR of the proposed F-DIC scheme under various OFDM symbols N_s for different NSR.

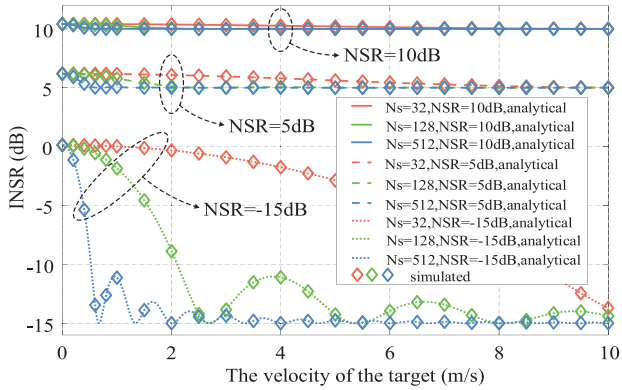

Fig. 3. INSR of the proposed F-DIC scheme under various target velocities for different NSR.

is defined as

$$\mathrm{INSR}\triangleq\frac{p_W+p_{\bar{N}}}{p_E}=\mathrm{ISR}+\mathrm{NSR}.\tag{35}$$

To depict the property of INSR more clearly, the influence of OFDM symbols and target velocity on the INSR with different NSRs is illustrated in Figs. 2 and 3, respectively.[2] The pictures show that the INSR goes down with the growth of the OFDM symbols and target velocity, respectively, except when the target velocity is zero, and then gradually coverages to the value of the corresponding NSR. This phenomenon indicates that as the OFDM symbol or target velocity rises, the residual interference decreases and drops slightly lower than the noise level. In other words, the thermal noise is the dominant unwanted component after the proposed method when the symbol or target velocity is sufficiently large. Also, it can be known from both figures that larger noise power leads to more rapid convergence. Considering that the radar echo (useful signal) is usually lower than the noise level, particularly if the target is not near the receiver (i.e., NSR >0 dB for sensing system), both pictures show that the residual interference has a little influence on the useful signal as long as the OFDM symbol or target velocity is adequate. Note

[2]Note that some simulation parameters are from Table II in Section V

that in both figures, due to the property of the sinc function and Fejér kernel, the INSR does not always decline as the increase of OFDM symbols $N_{\rm s}$ and target velocity v, especially in low NSR such as NSR $= -15$ dB. However, the whole trend of INSR is downward under this circumstance.

B. Interference Cancellation Performance

The interference cancellation performance of the proposed F-DIC scheme is analyzed in this subsection. When $N_{\rm c}$ is sufficiently large, based on the central limit theorem, the additive ICI term of the input signal can be approximated as a zero-mean complex Gaussian variable, associated with $I_{n,m} \sim \mathcal{CN}(0, \sigma_I^2)$, with the variance given by [27]

$$\sigma_I^2 = \mathrm{E}\left[|I_{n,m}|^2\right] = \frac{1}{N_{\rm c}} \sum_{n=0}^{N_{\rm c}-1} \left[\frac{(T_{\rm e} f_{\rm D})^2}{2} \sum_{k=0, k\neq n}^{N_{\rm c}-1} \frac{|\alpha|^2}{(k-n)^2} \right]. \quad (36)$$

Define the input signal to interference plus noise ratio (SINR) before F-DIC as the ratio of total input power of the useful signal to the power of the interference (including the static SI and ICI interference) plus noise, and P with the subscript represents the corresponding total power of the input signal. There is

$$\begin{aligned} \mathrm{SINR}_{\rm in} &\triangleq \frac{P_{\rm E}}{P_{\rm SI} + P_{\rm I} + P_{\rm N}} \\ &= \frac{|\alpha|^2 |\zeta|^2}{\sum_{q=0}^{Q-1} |\alpha_q|^2 + \sigma_I^2 + \sigma_N^2} = \frac{p_{\rm E}}{p_{\rm SI} + \phi}, \end{aligned} \quad (37)$$

in which $p_{\rm SI}$ is the average power at the single subcarrier of the static SI. Moreover, ϕ represents the sum of the additive ICI interference and the thermal noise.

As analyzed in Section IV-A, in order to show the influence of the residual interference, $(\bar{R}_{\rm TW})_{n,m}$ is defined as the output useful signal after F-DIC, which is written as

$$\left(\bar{R}_{\rm TW}\right)_{n,m} = (T_{\rm E})_{n,m} + \bar{W}_{n,m} = \alpha \zeta T^n \Omega_m X_{n,m}, \quad (38)$$

where $\Omega_m = F^m - \frac{1}{N_{\rm s}-1} \sum_{s=1}^{N_{\rm s}-1} F^s$ is the Doppler shift of the m-th OFDM symbol after the F-DIC method.

In addition, as $I_{n,m}^W$ in (28) is a linear combination of the ICI term $I_{n,m}$, there is $I_{n,m}^W \sim \mathcal{CN}(0, \frac{\sigma_I^2}{N_{\rm s}-1})$, and hence the output ICI term $\bar{I}_{n,m}$ still follows a zero-mean complex Gaussian distribution, i.e., $\bar{I}_{n,m} \sim \mathcal{CN}(0, \sigma_{\bar{I}}^2)$, with a variance of $\frac{N_{\rm s}}{N_{\rm s}-1}\sigma_I^2$.

Then, the output SINR after F-DIC is denoted as the ratio of output useful signal power to the output interference power plus noise power, which is

$$\mathrm{SINR}_{\rm out} \triangleq \frac{P_{\rm TW}}{P_{\bar{\rm I}} + P_{\bar{\rm N}}} = \frac{\frac{|\alpha|^2|\zeta|^2}{N_{\rm s}} \sum_{m=0}^{N_{\rm s}-1} |\Omega_m|^2}{\sigma_{\bar{I}}^2 + \sigma_{\bar{N}}^2} = \frac{p_{\rm TW}}{\frac{N_{\rm s}}{N_{\rm s}-1}\phi}, \quad (39)$$

where $p_{\rm TW}$ represents the average power at the single subcarrier of the output useful signal. Finally, the ICR for the proposed F-DIC method is obtained by the ratio of the output SINR to the input SINR, which can be written as

$$\begin{aligned} \mathrm{ICR} &\triangleq \frac{\mathrm{SINR}_{\rm out}}{\mathrm{SINR}_{\rm in}} \\ &= \frac{\frac{1}{N_{\rm s}} \sum_{m=0}^{N_{\rm s}-1} |\Omega_m|^2 \left(\sum_{q=0}^{Q-1} |\alpha_q|^2 + \sigma_I^2 + \sigma_N^2 \right)}{\sigma_{\bar{I}}^2 + \sigma_{\bar{N}}^2} \\ &= \frac{(p_{\rm SI} + \phi)\, p_{\rm TW}/p_{\rm E}}{\frac{N_{\rm s}}{N_{\rm s}-1}\phi}. \end{aligned} \quad (40)$$

Additionally, define the static SI to noise ratio (INR) as

$$\mathrm{INR} \triangleq \frac{P_{\rm SI}}{P_{\rm N}} = \frac{\sum_{q=0}^{Q-1} |\alpha_q|^2}{\sigma_N^2} = \frac{p_{\rm SI}}{\sigma_N^2}. \quad (41)$$

In the following, the effects of the number of OFDM symbols and the target velocity on the ICR will be discussed, respectively. Based on (40), two propositions can be made as follows.

Proposition 4.3: When the velocity of the moving target is not 0 m/s, and INR $\gg 1$, the ICR is improved with the increase of the number of OFDM symbols $N_{\rm s}$, and eventually approaches the INR.

Proof: As Proposition 4.1 indicates, the residual interference after F-DIC is negligible if the number of OFDM symbols is sufficiently large. The term representing $p_{\rm TW}/p_{\rm E}$ in (40) can be derived as

$$\frac{p_{\rm TW}}{p_{\rm E}} = \lim_{N_{\rm s}\to\infty} \frac{1}{N_{\rm s}} \sum_{m=0}^{N_{\rm s}-1} |\Omega_m|^2 = \lim_{N_{\rm s}\to\infty} \frac{1}{N_{\rm s}} \sum_{m=0}^{N_{\rm s}-1} |F^m|^2 = 1. \quad (42)$$

Therefore, when $N_{\rm s} \to \infty$, it yields

$$\begin{aligned} \lim_{N_{\rm s}\to\infty} \mathrm{ICR} &\approx \lim_{N_{\rm s}\to\infty} \frac{p_{\rm SI} + \sigma_N^2}{\frac{N_{\rm s}}{N_{\rm s}-1}\sigma_N^2} \\ &= \lim_{N_{\rm s}\to\infty} \frac{N_{\rm s}-1}{N_{\rm s}} (\mathrm{INR} + 1) \approx \mathrm{INR}, \end{aligned} \quad (43)$$

where the first approximation is made by taking into account that the ICI term is negligible when the target velocity is relatively low, and the last approximate equality holds because INR $\gg 1$.

It is common for INR $\gg 1$ since the power of the static SI is usually much higher than noise power. According to Proposition 4.3, to achieve promising interference cancellation performance, adequate OFDM symbols are required to be involved in the differential operation in the F-DIC method.

Proposition 4.4: The ICR will gradually decrease from the value approaching the INR with the decrease of the target speed. If the target speed drops to 0 m/s, the ICR also reduces to 0, meaning there is no useful signal output after F-DIC.

Proof: According to Proposition 4.2, as the target speed tends to 0 m/s, the power of residual interference increases, leading to the decrease of the power of output useful signal in (40), i.e., $\lim_{f_{\rm D}\to 0} p_{\rm TW} = 0$. And thus, there is $\lim_{f_{\rm D}\to 0} \mathrm{ICR} = 0$. ■

Note that the interference cancellation performance analysis can easily be extended to multi-moving targets for the independent property of the target echo signals. Only the average power of the useful signal before and after the F-DIC, i.e., $p_{\rm E}$ and $p_{\rm TW}$, need to be rewritten as the average power sum of the moving target signals.

C. Target Detection Performance

In this subsection, the detection performance of OFDM ISAC systems with F-DIC is analyzed based on the Neyman-Pearson criterion. To sense the velocity and the range of the target, a periodogram-based estimation algorithm is adopted in the OFDM radar [30]. The random data symbols in the output signal after F-DIC are mitigated by the element-wise division, and the data-normalized output is $(R_{\mathrm{D}})_{n,m} = \bar{R}_{n,m}/X_{n,m}$. Then, a DFT is performed on each column of the normalized output matrix $\mathbf{R}_{\mathrm{D}}$ to obtain the Doppler estimate, while an inverse discrete Fourier transform (IDFT) is performed on each row of it to obtain the delay estimate in the OFDM radar [4], [30]. Define the delay-Doppler bin of the target is $(\hat{n}, \hat{m})$, where $\hat{n}$, $\hat{m}$ are both integers and $\hat{n} \in \{0, \ldots, N_{\mathrm{c}} - 1\}$, $\hat{m} \in \{\lfloor -N_{\mathrm{s}}/2 \rfloor, \ldots, \lfloor N_{\mathrm{s}}/2 \rfloor - 1\}$. Therefore, the value at $(\hat{n}, \hat{m})$ can be written as

$$\Lambda_{\hat{n},\hat{m}} = \left(\mathbf{F}_{N_{\mathrm{c}}}^{H} \mathbf{R}_{\mathrm{D}} \mathbf{F}_{N_{\mathrm{s}}}\right)_{\hat{n},\hat{m}} = \hat{T}_{\mathrm{E}} + \hat{W} + \hat{I} + \hat{N}, \tag{44}$$

where

$$\begin{aligned}\hat{T}_{\mathrm{E}} &= \frac{\alpha\zeta}{\sqrt{N_{\mathrm{c}}N_{\mathrm{s}}}} \sum_{i=0}^{N_{\mathrm{c}}-1} \left(TW^{-\hat{n}}\right)^{i} \sum_{h=0}^{N_{\mathrm{s}}-1} \left[F(W_{\mathrm{s}})^{\hat{m}}\right]^{h} \\ &= \alpha\zeta\sqrt{N_{\mathrm{c}}N_{\mathrm{s}}},\end{aligned} \tag{45}$$

$$\hat{W} = \frac{1}{\sqrt{N_{\mathrm{c}}N_{\mathrm{s}}}} \sum_{h=0}^{N_{\mathrm{s}}-1} \sum_{i=0}^{N_{\mathrm{c}}-1} \frac{\bar{W}_{i,h}}{X_{i,h}} W^{-\hat{n}i} (W_{\mathrm{s}})^{\hat{m}h}, \tag{46}$$

$$\hat{I} = \frac{1}{\sqrt{N_{\mathrm{c}}N_{\mathrm{s}}}} \sum_{h=0}^{N_{\mathrm{s}}-1} \sum_{i=0}^{N_{\mathrm{c}}-1} \frac{\bar{I}_{i,h}}{X_{i,h}} W^{-\hat{n}i} (W_{\mathrm{s}})^{\hat{m}h}, \tag{47}$$

$$\hat{N} = \frac{1}{\sqrt{N_{\mathrm{c}}N_{\mathrm{s}}}} \sum_{h=0}^{N_{\mathrm{s}}-1} \sum_{i=0}^{N_{\mathrm{c}}-1} \frac{\bar{N}_{i,h}}{X_{i,h}} W^{-\hat{n}i} (W_{\mathrm{s}})^{\hat{m}h}, \tag{48}$$

where $W_{\mathrm{s}} = e^{-j2\pi/N_{\mathrm{s}}}$. The first term $\hat{T}_{\mathrm{E}}$ represents the value of the useful signal at the expected target bin after the OFDM radar processing. Note that $TW^{-\hat{n}} = 1$ and $F(W_{\mathrm{s}})^{\hat{m}} = 1$ in (45). For the second term, which is the residual interference after the OFDM radar processing, substituting (27) into (46) yields

$$\begin{aligned}\hat{W} &= \frac{-\alpha\zeta}{(N_{\mathrm{s}}-1)\sqrt{N_{\mathrm{c}}N_{\mathrm{s}}}} \sum_{i=0}^{N_{\mathrm{c}}-1} \left(TW^{-\hat{n}}\right)^{i} \sum_{h=0}^{N_{\mathrm{s}}-1} \left[\sum_{s=1}^{N_{\mathrm{s}}-1} F^{s} (W_{\mathrm{s}})^{\hat{m}h}\right] \\ &= \frac{-\alpha\zeta N_{\mathrm{c}}}{(N_{\mathrm{s}}-1)\sqrt{N_{\mathrm{c}}N_{\mathrm{s}}}} \left\{ \sum_{h=1}^{N_{\mathrm{s}}-1} \left[F(W_{\mathrm{s}})^{\hat{m}}\right]^{h} + \sum_{s=1}^{N_{\mathrm{s}}-1} F^{s} \right. \\ &\quad \left. + \sum_{h=1}^{N_{\mathrm{s}}-1} \left[\sum_{s=1,\ s\neq h}^{N_{\mathrm{s}}-1} F^{s} (W_{\mathrm{s}})^{\hat{m}h}\right] \right\} \\ &= \frac{-\alpha\zeta N_{\mathrm{c}}}{\sqrt{N_{\mathrm{c}}N_{\mathrm{s}}}} \left(1 + \frac{1}{N_{\mathrm{s}}-1} \sum_{s=1}^{N_{\mathrm{s}}-1} F^{s} + \frac{1}{N_{\mathrm{s}}-1} \sum_{h=1}^{N_{\mathrm{s}}-1} \sum_{s=1,s\neq h}^{N_{\mathrm{s}}-1} F^{s-h}\right).\end{aligned} \tag{49}$$

Since the ICI term $\hat{I}$ and the noise term $\hat{N}$ are the outputs of a DFT and an IDFT, they both perform on zero-mean complex Gaussian variables, with $\hat{I} \sim \mathcal{CN}(0, \sigma_{\hat{I}}^2)$ and $\hat{N} \sim \mathcal{CN}(0, \sigma_{\hat{N}}^2)$, due to the linearity of the DFT and the IDFT, and the normalized data symbols.

According to (44), depending on whether the moving target exists or not, the output signal after F-DIC and radar processing can be expressed as

$$\mathcal{H}_1 : \Lambda_{\hat{n},\hat{m}} = \hat{T}_{\mathrm{E}} + \hat{W} + \hat{I} + \hat{N}, \quad \mathcal{H}_0 : \Lambda_{\hat{n},\hat{m}} = \hat{N}. \tag{50}$$

This is a binary hypothesis testing problem, of which a linear detector is adopted as $z = |\Lambda_{\bar{n},\bar{m}}| \underset{H_0}{\overset{H_1}{\gtrless}} \Gamma$, with Γ denoting the detection threshold.

Under the hypothesis $\mathcal{H}_0$, z is Rayleigh distributed since $\hat{N} \sim \mathcal{CN}(0, \sigma_{\hat{N}}^2)$, and its probability density function (PDF) can be represented as [31]

$$f_0(z) = \frac{2z}{\sigma_{\hat{N}}^2} \exp\left(-\frac{z^2}{\sigma_{\hat{N}}^2}\right), \ z > 0. \tag{51}$$

Then, the probability of the false alarm is calculated as

$$P_{\mathrm{FA}} = \int_{\Gamma}^{+\infty} f_0(z)\, dz = \exp\left(-\frac{\Gamma^2}{\sigma_{\hat{N}}^2}\right). \tag{52}$$

Hence, for a constant P_{FA}, the detection threshold can be obtained by (52) as $\Gamma = \sigma_{\hat{N}}\sqrt{-\ln P_{\mathrm{FA}}}$.

When the target exists, i.e., under the hypothesis $\mathcal{H}_1$, z follows Rician distribution and its PDF is

$$f_1(z) = \frac{2z}{\sigma^2} \exp\left(-\frac{z^2 + \left|\hat{R}_{\mathrm{TW}}\right|^2}{\sigma^2}\right) I_0\left(\frac{2z\left|\hat{R}_{\mathrm{TW}}\right|}{\sigma^2}\right), z > 0, \tag{53}$$

where $\hat{R}_{\mathrm{TW}} \triangleq \hat{T}_{\mathrm{E}} + \hat{W}$, $\sigma^2 = \frac{N_{\mathrm{s}}}{N_{\mathrm{s}}-1}\phi = \sigma_{\hat{I}}^2 + \sigma_{\hat{N}}^2$, and $I_0(\cdot)$ is the modified Bessel function of the first kind [31]. The power of $\hat{R}_{\mathrm{TW}}$ can be written as

$$\left|\hat{R}_{\mathrm{TW}}\right|^2 = \left|\hat{T}_{\mathrm{E}} + \hat{W}\right|^2 = |\alpha|^2 |\zeta|^2 N_{\mathrm{c}} \Upsilon = p_{\mathrm{E}} N_{\mathrm{c}} \Upsilon, \tag{54}$$

where

$$\Upsilon = \left|\sqrt{N_{\mathrm{s}}} - \frac{1}{\sqrt{N_{\mathrm{s}}}} \left(1 + \frac{1}{N_{\mathrm{s}}-1} \sum_{s=1}^{N_{\mathrm{s}}-1} F^{s} + \frac{1}{N_{\mathrm{s}}-1} \sum_{h=0}^{N_{\mathrm{s}}-1} \sum_{s=1,s\neq h}^{N_{\mathrm{s}}-1} F^{s-h}\right)\right|^2. \tag{55}$$

Finally, the detection probability is given by

$$\begin{aligned}P_{\mathrm{D}} &= \int_{\Gamma}^{+\infty} f_1(z)\, dx = Q_{\mathrm{M}}\left(\sqrt{\frac{2\left|\hat{R}_{\mathrm{TW}}\right|^2}{\sigma^2}}, \sqrt{\frac{2|\Gamma|^2}{\sigma^2}}\right) \\ &= Q_{\mathrm{M}}\left(\sqrt{2\mathrm{SINR}_{\mathrm{radar}}}, \sqrt{\frac{-2\sigma_{\hat{N}}^2 \ln P_{\mathrm{FA}}}{\sigma_{\hat{I}}^2 + \sigma_{\hat{N}}^2}}\right),\end{aligned} \tag{56}$$

where $Q_{\mathrm{M}}(a, b)$ is the Marcum's Q function [31] and the SINR at the expected delay-Doppler bin after radar processing is defined as $\mathrm{SINR}_{\mathrm{radar}} = |\hat{R}_{\mathrm{TW}}|^2/\sigma^2$.

Similar to the interference cancellation performance analysis, in the following, the effects of the F-DIC methods on the

detection probability will be discussed through the length of differential operation and the target velocity.

Proposition 4.5: If the velocity of the target is not 0 m/s, the detection performance of OFDM sensing systems with F-DIC is improved with the increase of the number of OFDM symbols N_{s}.

Proof: It is known from Proposition 4.1 that $\lim_{N_{\mathrm{s}}\to\infty} \bar{W}_{n,m} = 0$. Additionally, there is $\lim_{N_{\mathrm{s}}\to\infty} \hat{W} = 0$ considering the linear transformation property of DFT and IDFT, and also the normalized data symbols. Therefore, when the number of OFDM symbols is relatively large, it yields $\Upsilon \approx N_{\mathrm{s}}$, resulting in $|\hat{R}_{\mathrm{TW}}|^2 \approx p_{\mathrm{E}} N_{\mathrm{c}} N_{\mathrm{s}}$. $N_{\mathrm{c}}N_{\mathrm{s}}$ is defined as the processing gain of the OFDM radar [4], [8]. With the increase of N_{s}, the processing gain is increased, improving the detection performance for the OFDM sensing system. ■

According to the property of Marcum's Q function, there is $P_{\mathrm{D}} \to 1$ when N_{s} is sufficiently large in (56).

Proposition 4.6: The detection probability will decrease with the decrease of the target velocity. If the target speed drops to 0 m/s, the detection probability P_{D} also reduces to 0, which means that the target echo signal is suppressed by F-DIC and the radar processing gain for this static target is 0.

Proof: If the velocity of the target tends to 0 m/s, i.e., $f_{\mathrm{D}} \to 0$, (55) becomes

$$\lim_{f_{\mathrm{D}}\to 0} \Upsilon = \left| \sqrt{N_{\mathrm{s}}} - \frac{1}{\sqrt{N_{\mathrm{s}}}} \left[1 + \frac{1}{N_{\mathrm{s}}-1} (N_{\mathrm{s}}-1) + \frac{1}{N_{\mathrm{s}}-1} (N_{\mathrm{s}}-1)(N_{\mathrm{s}}-2) \right] \right|^2 = 0. \tag{57}$$

Hence, it yields $\lim_{f_{\mathrm{D}}\to 0} |\hat{R}_{\mathrm{TW}}|^2 = \lim_{f_{\mathrm{D}}\to 0} \mathrm{SINR}_{\mathrm{radar}} = 0$, and then $\lim_{f_{\mathrm{D}}\to 0} P_{\mathrm{D}} = 0$. ■

D. Computational Complexity

The proposed F-DIC scheme has quite low complexity, which is comparable to the TD blind known interference cancellation scheme in [24]. In this subsection, the number of complex multiplications is utilized as a metric to assess the complexity of the proposed method and some classical interference cancellation methods in both the time domain [9] and frequency domain [21]. This metric selection is justified by the widespread use of complex multiplications in signal processing methods and their resource-intensive nature, particularly in typical field programmable gate array (FPGA) units [32].

Considering the element-wise division operation at the beginning of the OFDM radar processing, the proposed F-DIC scheme can utilize this element-wise division before the interference cancellation steps. In this manner, the complex multiplication operations related to the data symbols are able to be omitted in the subsequent processing procedures of the F-DIC method, resulting in no additional complex multiplications in the differential operations. The output is $(R_{\mathrm{D}})_{n,m}$, which can be used for further OFDM radar processing in (44). In addition, it is possible to calculate the reciprocal of the data symbols offline due to the limited symbol set of $X_{n,m}$, which is drawn from pre-defined constellations such as QPSK. Therefore, the proposed F-DIC method only requires $N_{\mathrm{c}}N_{\mathrm{s}}$ times complex multiplications at the element-wise division in whole procedures. If FFT and inverse fast Fourier transform (IFFT) are taken into consideration, the computational complexity of the proposed F-DIC is $N_{\mathrm{c}}N_{\mathrm{s}}\log_2 N_{\mathrm{c}} + N_{\mathrm{c}}N_{\mathrm{s}}$.

TABLE I
COMPUTATIONAL COMPLEXITY OF DIFFERENT ALGORITHMS

Algorithm	Complex multiplications
T-LS	$M^2\log_2 M + (K+1)M^2 + 2KM$
T-RLS	$4M^2N + 4(M+2)N + MN_{\mathrm{c}}N_{\mathrm{s}}$
T-NLMS	$3(M+1)N + MN_{\mathrm{c}}N_{\mathrm{s}}$
F-LS	$N_{\mathrm{c}}N_{\mathrm{s}}\log_2 N_{\mathrm{c}} + 3N_{\mathrm{c}}(N_{\mathrm{s}}+1)$
F-RLS	$N_{\mathrm{c}}N_{\mathrm{s}}\log_2 N_{\mathrm{c}} + 11N_{\mathrm{c}}N_{\mathrm{s}}$
F-NLMS	$N_{\mathrm{c}}N_{\mathrm{s}}\log_2 N_{\mathrm{c}} + 3N_{\mathrm{c}}N_{\mathrm{s}}$
F-DIC	$N_{\mathrm{c}}N_{\mathrm{s}}\log_2 N_{\mathrm{c}} + N_{\mathrm{c}}N_{\mathrm{s}}$

The computational complexity of F-LS [21] is calculated firstly for comparison. The output signal vector of the F-LS method can be written as

$$\bar{\boldsymbol{r}}_n = \boldsymbol{r}_n - \boldsymbol{x}_n \left(\boldsymbol{x}_n^H \boldsymbol{x}_n\right)^{-1} \boldsymbol{x}_n^H \boldsymbol{r}_n, \tag{58}$$

where $\boldsymbol{r}_n = [R_{n,0}, R_{n,1}, \ldots, R_{n,N_{\mathrm{s}}-1}]^T$ is the FD received signal vector at the n-th subcarrier and $\boldsymbol{x}_n = [X_{n,0}, X_{n,1}, \ldots, X_{n,N_{\mathrm{s}}-1}]^T$ is the data symbol vector at the n-th subcarrier. The complex multiplications when calculating $\boldsymbol{x}_n^H \boldsymbol{x}_n$ are N_{s}. It is worth noting that the reciprocal calculation of a complex number equals one real number division, two real multiplications, and one complex multiplication. In the FPGA, the resource usage of a real number divider is approximately equal to that of a complex multiplier [32]. Thus, in this complexity computation, the reciprocal of a complex number is regarded as two complex multiplications, and the complex multiplications of variable $a_n = (\boldsymbol{x}_n^H \boldsymbol{x}_n)^{-1}$ are 2. Then the number of complex multiplications is N_{s} for variable $b_n = \boldsymbol{x}_n^H \boldsymbol{r}_n$, 1 for variable $c_n = a_n b_n$ and N_{s} for $\boldsymbol{x}_n c_n$. Hence, the overall complex multiplications on N_{c} subcarriers of the F-LS algorithm are $3N_{\mathrm{c}}(N_{\mathrm{s}}+1)$, and $N_{\mathrm{c}}N_{\mathrm{s}}\log_2 N_{\mathrm{c}} + 3N_{\mathrm{c}}(N_{\mathrm{s}}+1)$ considering FFT and IFFT. Following the similar calculation approach, the computational complexity of the other two FD interference cancellation methods [21], i.e., frequency-domain recursive least squares (F-RLS) and frequency-domain normalized least mean squares (F-NLMS), are calculated and listed in Table I. The iteration times of those two adaptive filter algorithms are both N_{s}.

The computational complexity of three conventional TD interference cancellation methods [9], which are time-domain least squares (T-LS), time-domain recursive least squares (T-RLS) and time-domain normalized least mean squares (T-NLMS), are also calculated and listed in Table I for comparison, where M is the order of the transversal filter deciding the maximum cancellation range. Additionally, $K = (N_{\mathrm{c}} + N_{\mathrm{cp}})N_{\mathrm{s}}$ is the length of the received signal, with N_{cp} being the number of the CP, and N is the number of iterations for the T-RLS and the T-NLMS. Note that not only estimation cost but also reconstruction cost are taken into account for all the adaptive filter algorithms both in the time and frequency domain.

The complex multiplications of FFT and IFFT in FD methods can be omitted in the OFDM system since the OFDM receiver has an FFT module for signal demodulation, and the processing for OFDM receivers is in the frequency domain. Furthermore, as aforementioned, the element-wise division operation is needed in the OFDM radar processing, which can also be multiplexed by the proposed F-DIC method. As a result, no additional complex multiplications are required when the F-DIC method is applied in the OFDM radar system. Besides, it can be observed from Table I that, different from the TD algorithms, the computational complexity of F-LS is smaller than that of F-RLS. The reason is that the multipath influence in the time domain is mapping into a complex value for one subcarrier, and the order M of the transversal filter in the frequency domain degrades to 1, significantly reducing the computational complexity of the F-LS algorithm.

E. Comparison With F-LS

This subsection provides the output signal comparison between the proposed F-DIC method and the conventional F-LS method to illustrate that the proposed method achieves similar performance to the F-LS if N_s is sufficient and the OFDM symbols are unitary modulus modulated (e.g., QPSK or 8PSK). According to (16) and (58), the output signal after F-LS at a single subcarrier can be written as (see Appendix C for the proof)

$$\bar{R}_{n,m}^{\mathrm{F-LS}} = H_{n,m}^{M} X_{n,m} - \frac{X_{n,m}}{N_{\mathrm{s}}} \sum_{s=0}^{N_{\mathrm{s}}-1} H_{n,s}^{M} + N_{n,m} - \frac{X_{n,m}}{N_{\mathrm{s}}} \sum_{s=0}^{N_{\mathrm{s}}-1} \frac{N_{n,s}}{X_{n,s}}. \tag{59}$$

Following (14), the output signal after F-DIC in (26) can be rewritten as

$$\bar{R}_{n,m}^{\mathrm{F-DIC}} = H_{n,m}^{M} X_{n,m} - \frac{X_{n,m}}{N_{\mathrm{s}}-1} \sum_{s=1}^{N_{\mathrm{s}}-1} H_{n,s}^{M} + N_{n,m} - \frac{X_{n,m}}{N_{\mathrm{s}}-1} \sum_{s=1}^{N_{\mathrm{s}}-1} \frac{N_{n,s}}{X_{n,s}}. \tag{60}$$

It can be seen from (59) and (60) that the two interference cancellation schemes have similar output signals when the OFDM symbols are unitary modulus modulated. The difference is that the residual interference of the F-LS method is the average value of all the OFDM symbols (N_{s} in all) at the same subcarrier while the residual interference of the proposed F-DIC method is the average value of the indexed 1 to $N_{\mathrm{s}}-1$ OFDM symbols. In other words, the proposed F-DIC does not add the indexed 0 OFDM symbol into the average value calculation. Based on (59) and (60), the output difference of the two methods is

$$\bar{R}_{n,m}^{\mathrm{F-DIC}} - \bar{R}_{n,m}^{\mathrm{F-LS}} = \frac{1}{N_{\mathrm{s}}} \left(H_{n,0}^{M} X_{n,m} - \frac{X_{n,m}}{N_{\mathrm{s}}-1} \sum_{s=1}^{N_{\mathrm{s}}-1} H_{n,s}^{M} + \frac{N_{n,0}}{X_{n,0}} - \frac{X_{n,m}}{N_{\mathrm{s}}-1} \sum_{s=1}^{N_{\mathrm{s}}-1} \frac{N_{n,s}}{X_{n,s}} \right) = \frac{1}{N_{\mathrm{s}}} \bar{R}_{n,0}^{\mathrm{F-DIC}}. \tag{61}$$

TABLE II
OFDM ISAC SYSTEM PARAMETER SETTINGS AT 24 GHZ ISM BAND

Parameter	Meaning	Value
f_{c}	Carrier frequency	24 GHz
λ	Wavelength	0.0125 m
N_{c}	Number of subcarriers	2048
Δf	Subcarrier spacing	60 kHz
T_{e}	OFDM data symbol duration	16.67 μs
T_{cp}	CP duration	1.56 μs
T_{s}	Total OFDM symbol duration	18.23 μs
B	Signal bandwidth	122.88 MHz
N_{s}	Number of OFDM symbols	128
N_0	Receiver noise floor	-93.1 dBm
NF	Receiver noise figure	6 dB
ΔR	Radar range resolution	1.22 m
$R_{\max}$	Maximum detection range	2500 m
Δv	Radar velocity resolution	2.68 m/s
$v_{\max}$	Maximum detection velocity	75 m/s

Therefore, the normalized mean square error (NMSE) in terms of the F-DIC method can be denoted as

$$\gamma = \frac{\mathrm{E}\left[\left|\bar{R}_{n,m}^{\mathrm{F-DIC}} - \bar{R}_{n,m}^{\mathrm{F-LS}}\right|^2\right]}{\mathrm{E}\left[\left|\bar{R}_{n,m}^{\mathrm{F-DIC}}\right|^2\right]} = \frac{\frac{1}{N_{\mathrm{s}}^2}\mathrm{E}\left[\left|\bar{R}_{n,0}^{\mathrm{F-DIC}}\right|^2\right]}{\mathrm{E}\left[\left|\bar{R}_{n,m}^{\mathrm{F-DIC}}\right|^2\right]} \approx \frac{1}{N_{\mathrm{s}}^2} \frac{\mathrm{E}\left[\left|\bar{R}_{n,m}^{\mathrm{F-DIC}}\right|^2\right]}{\mathrm{E}\left[\left|\bar{R}_{n,m}^{\mathrm{F-DIC}}\right|^2\right]} = \frac{1}{N_{\mathrm{s}}^2}, \tag{62}$$

where $\mathrm{E}[|\cdot|^2]$ represents the average power at signal subcarrier. Moreover, the approximation in (62) is made by assuming that the average subcarrier power of the OFDM symbol indexed 0 is similar to that of all OFDM symbols. The NMSE γ shows the deviation extent between the F-LS and F-DIC output signals. When N_{s} is large, there is $\gamma \approx 0$, which means the F-LS and F-DIC output signals are almost identical, and the deviation between them can be ignored.

As for the other two FD adaptive filter methods, F-RLS and F-NLMS, their interference cancellation performances are also close to the F-LS method as long as the iteration times are adequately large and the iteration parameters are set up correctly [33].

V. NUMERICAL RESULTS AND DISCUSSIONS

In this section, some numerical and simulation results are provided to evaluate the performance of the proposed F-DIC method. Moreover, the computational complexity and interference cancellation performance of the proposed scheme are compared with the conventional methods.

A. Simulation Environment

A set of 24 GHz industrial scientific medical (ISM) band-based parameters is given in Table II for the following simulations. The subcarrier spacing is set to be 60 kHz, the smallest one in standard millimeter-wave frequency bands of the 5G New Radio [8]. Moreover, QPSK modulation is adopted in the system.

TABLE III
INTERFERENCE CHANNEL PARAMETERS FOR SIMULATION

Type	Range	Time delay (s)	Normalized power
Direct path	$1\Delta R$	4.0690×10^{-9}	1024/1365
Multipath 1	$6\Delta R$	4.8828×10^{-8}	256/1365
Multipath 2	$11\Delta R$	8.9518×10^{-8}	64/1365
Multipath 3	$16\Delta R$	1.3021×10^{-7}	16/1365
Multipath 4	$21\Delta R$	1.7090×10^{-7}	4/1365
Multipath 5	$26\Delta R$	2.1159×10^{-7}	1/1365

To maintain the orthogonality of the subcarriers, the Doppler shift at the user's communication receiver must be smaller than $0.1\Delta f$ [4], [5], which means the Doppler shift of the target echo signal at the BS sensing receiver should satisfy $f_{\mathrm{D}} \leq 0.2\Delta f$ when the sensed target is also a CU. The reason is that the target echo signal undergoes a two-way propagation, while the communication signal undergoes a one-way propagation. Therefore, the maximum relative velocity is $v_{\max} = cf_{\mathrm{D,max}}/(2f_{\mathrm{c}}) = 75\ \mathrm{m/s}$, where c is the speed of light and $f_{\mathrm{D,max}} = 0.2\Delta f = 12$ kHz. According to the symbol duration, the maximum sensing range of the radar is $R_{\max} = cT_{\mathrm{e}}/2 \approx 2500\ \mathrm{m}$. In addition, the range resolution is calculated as $\Delta R = c/(2B) = 1.22\ \mathrm{m}$, while the velocity resolution is $\Delta v = 2.68\ \mathrm{m/s}$ for $N_s = 128$.

The channel gain for the target echo signal is modeled as [4], [30], [31]

$$|\alpha|^2 = \frac{P_{\mathrm{T}} G_{\mathrm{T}} G_{\mathrm{R}} \sigma_{\mathrm{RCS}} \lambda^2}{(4\pi)^3 R^4}, \tag{63}$$

with P_{T}, G_{T}, G_{R} being the transmission power, the transmitter gain, and the receiver gain, respectively, σ_{RCS} denoting the radar cross section (RCS) of the target, and R representing the distance between the target and the BS receiver. The parameters are given as $P_{\mathrm{T}}G_{\mathrm{T}} = 20\,\mathrm{dBm}$, $G_{\mathrm{R}} = 20\,\mathrm{dBi}$, and $\sigma_{\mathrm{RCS}} = 3.5\,\mathrm{dBsm}$ (which is the RCS of a car at 24 GHz measured in [34]).

The interference channel parameters are listed in Table III. The parameter range in the first row represents the propagation distance of the direct SI signal, while the rest rows represent the distance between the static reflector and the BS. It can be seen that the sum of the normalized power factors is 1, and the power gain decreases by 6 dB for the adjacent paths.

Note that the number of trials for the Monte Carlo method is fifty thousand to obtain the numerical results. Besides, unless otherwise specified, the parameters are adopted in the above settings in the following simulations.

B. Results and Discussions

Fig. 4 compares the range-velocity radar images for the sensing receiver with and without F-DIC in the scenario with the direct SI and the multipath interference. The total INR of the interference is 35 dB, and the interpolation factor is 8. The rectangular window is used in Fig. 4(a) and 4(a), while the Hamming window is used in Fig. 4(c) and 4(c). Assume that there are 6 point scatterers to be sensed, whose range and velocity are listed in Table IV. For the sake of observation, note that the channel coefficients for all targets in Fig. 4 are assumed to be identical regardless of the distance and the RCS of the targets,

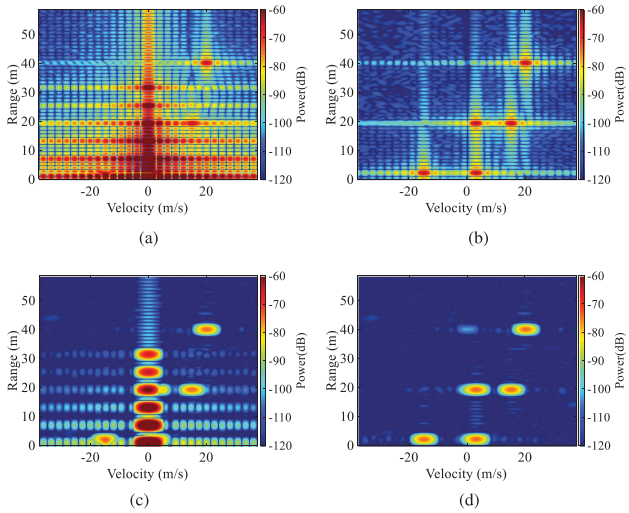

Fig. 4. Range-velocity images using different window functions for interference and six targets (one of which is a static target) with the same channel gain (for observation). (a) Rectangular window without F-DIC. (b) Rectangular window with F-DIC. (c) Hamming window without F-DIC. (d) Hamming window with F-DIC.

TABLE IV
RANGE AND VELOCITY OF THE SIX TARGETS IN FIG. 4

Target index	1	2	3	4	5	6
Range	2 m	2 m	20 m	20 m	32 m	40 m
Velocity	-15 m/s	3 m/s	3 m/s	15 m/s	0 m/s	20 m/s

and the signal-to-noise ratios of the received target echo signals are all set to 0 dB.

It can be clearly observed from Fig. 4(a) and (c) that after radar processing, the direct SI is a strong static target around the BS, while its sidelobes caused by the window function introduce severe interference across a wide range of distances at a low velocity and at a close range for variable velocities, which influence the detection of true weaker low-speed targets as well as close-range targets [5]. Similarly, it can be observed for the multipath interference that their sidelobes influence a wide range of distances at a low velocity and at a range around the stationary reflectors for variable velocities. Therefore, it is necessary to cancel the static SI to improve the sensing performance. As shown in Fig. 4(b) and (d), the proposed F-DIC method can effectively cancel the static SI while extracting the moving target echoes, despite the influence of the static SI on some of them (i.e., those with a low velocity, around the interference reflectors or BS). It is worth noting that the echo signal of target 5, a static target 32 m away from the BS, cannot be correctly extracted by the proposed F-DIC, for its velocity is zero. However, as shown in [5], it is acceptable since the SI usually covers the static targets in real roadside measurement scenarios.

To show the computational complexity of the proposed F-DIC method, Table V gives the number of complex multiplication operations required by the F-DIC and the classical TD/FD interference cancellation methods in [9], [21]. The results in Table V are calculated based on Table I, with $M = 24$ and $N = N_{\mathrm{c}}$ (which are also used for the following comparison

TABLE V
NUMBER OF COMPLEX MULTIPLICATION OPERATIONS FOR DIFFERENT ALGORITHMS WITH $M = 24$ AND $N = N_c$

Algorithm	Complex multiplications
T-LS	1.79×10^8
T-RLS	1.12×10^7
T-NLMS	6.45×10^6
F-LS	7.93×10^5
F-RLS	2.88×10^6
F-NLMS	7.86×10^5
F-DIC	2.62×10^5

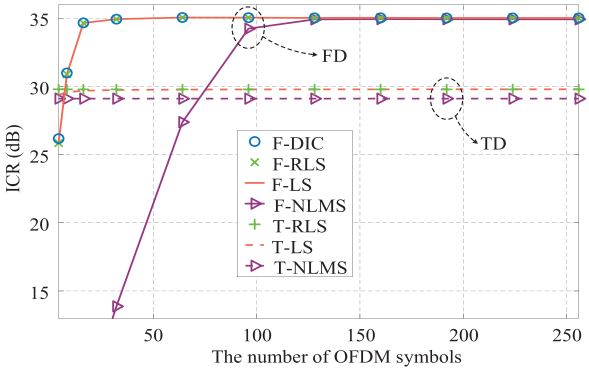

Fig. 5. Interference cancellation performance of the proposed F-DIC scheme and the conventional TD/FD methods under various OFDM symbols N_s, where $R = 50\Delta R$, INR = 35 dB, and $v = 15$ m/s.

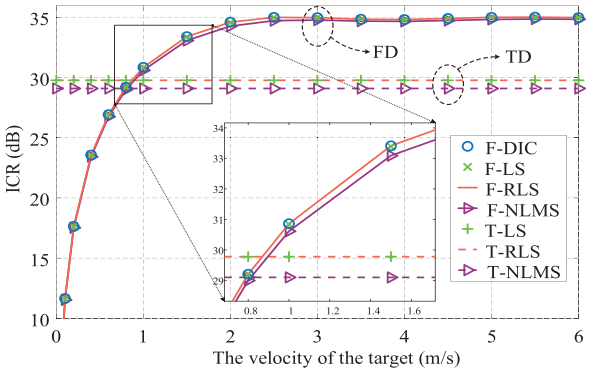

Fig. 6. Interference cancellation performance of the proposed F-DIC scheme and the conventional TD/FD methods under various target velocities, where $R = 50\Delta R$, INR = 35 dB, and $N_s = 128$.

simulations). Note that the consumption of FFT and IFFT in FD methods is omitted. Table V identifies that the complexity of FD methods is lower than TD methods, especially when omitting the FFT and IFFT consumption. More importantly, the proposed F-DIC method has promising low complexity, and its number of complex multiplication operations is one-third of that of the F-NLMS method, which has the lowest complex multiplication consumption in the classical TD/FD interference cancellation methods.

Figs. 5– 7 compare the interference cancellation performance of the proposed F-DIC method and conventional TD/FD methods. As aforementioned, the order of the transversal filter of the three TD methods is $M = 24$, while the number of iterations

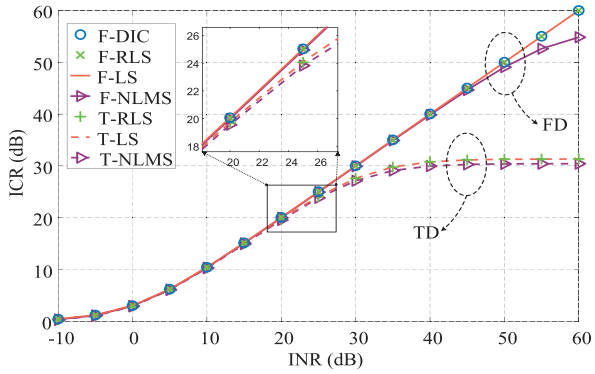

Fig. 7. Interference cancellation performance of the proposed F-DIC scheme and the conventional TD/FD methods under different INR, where $R = 50\Delta R$, $N_s = 128$, and $v = 15$ m/s.

for the two TD adaptive filter methods is $N = N_c$. The distance between the target and the BS receiver is $R = 50\Delta R$. It is worth noting that one static reflector that causes Multipath 5 in Table III is located outside of the maximum cancellation range for TD methods, i.e., the transversal filter order is not high enough to cover all the multipaths.

Fig. 5 illustrates the interference cancellation performance of the proposed F-DIC scheme and the conventional TD/FD methods under various OFDM symbols N_s. The total INR of the SI is 35 dB, and the target velocity is $v = 15$ m/s. It can be seen that the TD methods are almost not influenced by the number of OFDM symbols. Only the performance of T-LS slightly loses at small N_s. Nevertheless, the TD methods cannot reach the maximum ICR because of the limited transversal filter order. In addition, T-NLMS does not achieve the same performance as T-LS and T-RLS methods due to insufficient iteration times. As for the FD methods, the ICR is improved with the growth of the number of OFDM symbols, and all the methods in the frequency domain can converge to the maximum ICR, i.e., 35 dB, which is mentioned in Proposition 4.3 for the F-DIC method. More importantly, Fig. 5 implies that although the proposed F-DIC scheme has the lowest computational complexity, it achieves the same performance as F-LS and F-RLS methods, which has been explained in Section IV-E. Furthermore, F-NLMS shows obviously poorer performance compared with the other FD methods. The reason is the same with the T-NLMS in the context of insufficient iteration times at small N_s.

The performance comparison is presented in Fig. 6 to show the impact of the target velocity on ICR. The total INR of the static SI is also 35 dB, and the number of OFDM symbols is 128. Same as Fig. 5, TD methods are not influenced by the velocity of the target because the target is located outside of the maximum cancellation range of the TD methods. However, the interference cancellation performance of the FD methods decreases when the target velocity decreases in a low-velocity scenario, and when the velocity is smaller than 0.8 m/s, the ICR of the FD methods is lower than that of the TD methods. Eventually, the ICR of the FD methods tends to zero as the target velocity approaches zero, as mentioned in Proposition 4.4. Note that as long as the target velocity is greater than 2 m/s, there

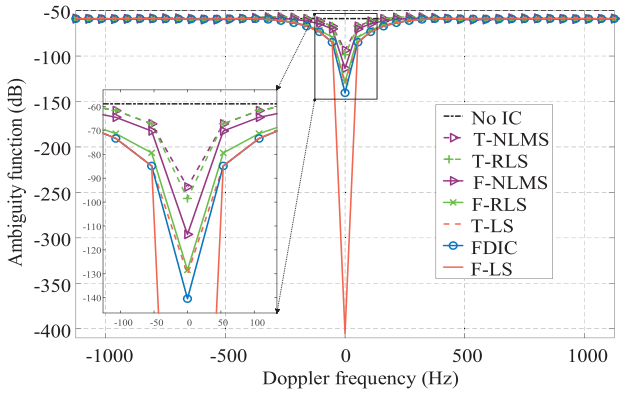

Fig. 8. Comparison of ambiguity function of the proposed F-DIC scheme and the conventional TD/FD methods under various Doppler frequency, where $R = 20\Delta R$ and $N_s = 128$.

is almost no performance distortion with the applied simulation parameters for the proposed F-DIC and the conventional F-LS/F-RLS methods. It can also be observed that the proposed F-DIC scheme has the same performance as F-LS and F-RLS methods.

Fig. 7 depicts the ICR performance of the proposed and conventional methods with different INR. The number of OFDM symbols is 128, and the target velocity is 15 m/s. It can be seen that the FD methods gradually outperform TD methods when INR $>$ 20 dB since the transversal filter order of TD methods does not cover all the multipaths. Additionally, the proposed F-DIC scheme has equivalent interference cancellation performance with F-LS and F-RLS methods as proved in Section IV-E while outperforming the F-NLMS method. Specifically, the F-NLMS method achieves almost the same ICR compared with the other FD methods when the INR is below 40 dB. However, when INR $=$ 60 dB, the F-NLMS method only cancels about 55 dB interference due to the insufficient iteration times, while the other FD methods, including the proposed F-DIC method, can still cancel the interference to the noise floor with ICR $=$ 60 dB.

The main purpose of the F-DIC method is to cancel the interference with zero (or with very small) velocity. Target echoes which have significant velocity should not be attenuated by it. From this point of view, frequency selectivity in the velocity dimension is important for the interference cancellation method of the sensing system (i.e., its ability to remove signal components with different velocities selectively) [9]. To verify the behavior of the proposed F-DIC methods and the conventional TD/FD methods, the slice of the ambiguity function at a fixed range [8], [9], [31], i.e., $R = 20\Delta R$, with different Doppler frequency is simulated in Fig. 8, where $N_s = 128$ and the interpolation factor is also 8. Note that the range is set to be $20\Delta R$, which is in the maximum cancellation range for the TD methods, and the black dash-dot line in the figure shows the ambiguity function of the OFDM radar system with no interference cancellation method. As shown in the picture, all the interference cancellation methods create notches around the zero Doppler frequency. And the FD methods have deeper zero Doppler notches than their corresponding TD methods. Moreover, the F-LS method has the deepest zero Doppler notch, which means it has the best

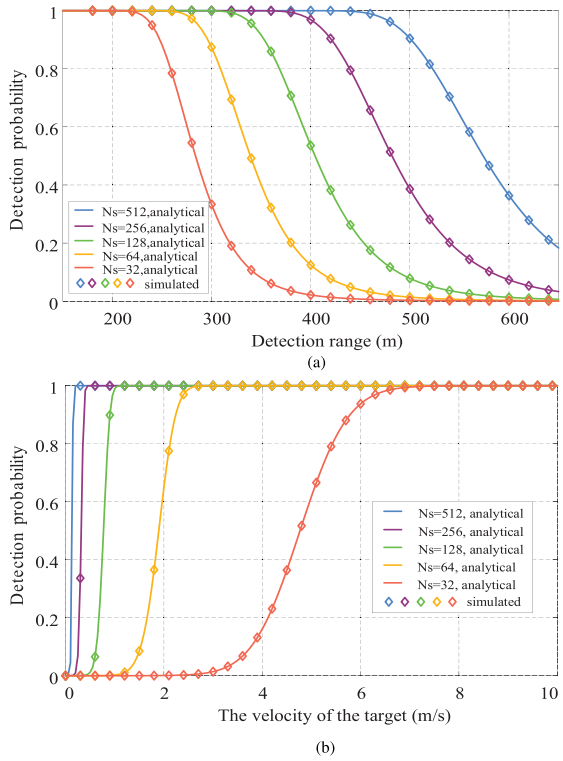

Fig. 9. Target detection performance of the OFDM radar using the proposed F-DIC scheme, where $P_{FA} = 10^{-4}$. (a) Detection performance of the OFDM radar under different detection ranges. (b) Detection performance of the OFDM radar under various target velocities.

interference cancellation performance at the zero Doppler frequency, while the proposed F-DIC has the second deepest notch. For digital static SI cancellation usually requiring a maximum of 60 dB cancellation capability, Fig. 8 implies that only T-LS, F-RLS, F-DIC, and F-LS have enough capability to cancel the static SI in the provided simulation situation.

Fig. 9 depicts the detection performance of OFDM ISAC systems with the proposed F-DIC method for $P_{FA} = 10^{-4}$ in (56). Fig. 9(a) shows the detection probability curves versus the detection range for different numbers of OFDM symbols with a target speed of 15 m/s. This figure indicates that the theoretical maximum detection range of the proposed system without miss detection based on the NP criterion is about 300 m (according to the green curve with $N_s = 128$). It is also shown that the detection performance is improved with the increase of the number of OFDM symbols N_s. This is because larger N_s results in larger OFDM radar processing gain, which equals $N_c N_s$. Additionally, the influence of the target velocity on the detection probability is presented in Fig. 9(b), which implies that the detection performance for low-speed targets is improved with the increase of the number of OFDM symbols. Moreover, if the target velocity is 0 m/s, the detection probability is also 0, as mentioned in Proposition 4.6. Note that the target is 200 m away from the BS. Furthermore, considering the velocity resolution, one should note that the F-DIC method will completely suppress the target echo with zero velocity. Other velocities, which are integer multiples of the velocity resolution, remain unaffected by the F-DIC method.

VI. Conclusion

By analyzing the characteristics of the received signal and leveraging the invariant property of the interference, a novel low-complexity F-DIC method is proposed for full-duplex OFDM ISAC systems to extract the moving target echo signals while canceling the static SI without the need for the CSI. After evaluating the influence of the residual interference of the proposed method, the interference cancellation performance is analyzed in terms of the ICR, and a closed-form expression for the target detection probability of the OFDM sensing system with F-DIC is derived under the NP criterion. In addition, the computational complexity is also presented to show that no additional complex multiplications are required for the proposed method by multiplexing the operations of the OFDM radar processing. Simulation results illustrate that the OFDM sensing system with F-DIC is capable of correctly detecting the moving targets, which the strong static SI will obscure in the range-velocity images without interference cancellation. Moreover, the proposed F-DIC method with promising low complexity performs similarly to the conventional FD LS/RLS interference cancellation method.

Appendix A
Proof of (9)

According to (8), the FD single path received signal is written as

$$\mathbf{R}_{\text{sig}} = \alpha \mathbf{F}_{N_\text{c}} \mathbf{D}_{(f_\text{D})} \mathbf{F}_{N_\text{c}}^H \left[\mathbf{X} \odot \mathbf{v}_\tau \mathbf{v}_f^H \right] \in \mathbb{C}^{N_\text{c} \times N_\text{s}}. \tag{64}$$

The received signal at the n-th subcarrier of the m-th OFDM symbol without ICI, i.e. assuming that $\mathbf{D}_{(f_\text{D})} \approx \mathbf{I}$, can be calculated as

$$\left(\dot{\mathbf{R}}_{\text{sig}} \right)_{n,m} = \left(\alpha \mathbf{X} \odot \mathbf{v}_\tau \mathbf{v}_f^H \right)_{n,m} = \alpha T^n F^m X_{n,m}. \tag{65}$$

In addition, based on the sum of the geometric sequence, the matrix $\mathbf{F}_{N_\text{c}} \mathbf{D}_{(f_\text{D})} \mathbf{F}_{N_\text{c}}^H$ is expressed as

$$\frac{1}{N_\text{c}} \begin{bmatrix} \frac{1-D^{N_\text{c}}}{1-D} & \frac{1-D^{N_\text{c}}}{1-DW^{-1}} & \cdots & \frac{1-D^{N_\text{c}}}{1-DW^{-(N_\text{c}-1)}} \\ \frac{1-D^{N_\text{c}}}{1-DW} & \frac{1-D^{N_\text{c}}}{1-D} & \cdots & \frac{1-D^{N_\text{c}}}{1-DW^{-(N_\text{c}-2)}} \\ \vdots & \vdots & \ddots & \vdots \\ \frac{1-D^{N_\text{c}}}{1-DW^{N_\text{c}-1}} & \frac{1-D^{N_\text{c}}}{1-DW^{N_\text{c}-2}} & \cdots & \frac{1-D^{N_\text{c}}}{1-D} \end{bmatrix},$$

where $W = e^{-j2\pi/N_\text{c}}$. Therefore, the single path received signal at the n-th subcarrier of the m-th OFDM symbol in (64) can be further derived as

$$\begin{aligned} \left(\mathbf{R}_{\text{sig}} \right)_{n,m} &= \left(\mathbf{F}_{N_\text{c}} \mathbf{D}_{(f_\text{D})} \mathbf{F}_{N_\text{c}}^H \dot{\mathbf{R}}_{\text{sig}} \right)_{n,m} \\ &= \frac{\alpha}{N_\text{c}} \sum_{k=0}^{N_\text{c}-1} \frac{1-D^{N_\text{c}}}{1-DW^{-k+n}} T^k F^m X_{k,m} \\ &= \alpha \frac{1-D^{N_\text{c}}}{N_\text{c}(1-D)} T^n F^m X_{n,m} \\ &\quad + \sum_{k=0,\ k\neq n}^{N_\text{c}-1} \alpha \frac{1-D^{N_\text{c}}}{N_\text{c}(1-DW^{-k+n})} X_{k,m} T^k F^m. \end{aligned} \tag{66}$$

Appendix B
Proof of Lemma IV.1

If $f_\text{D} = 0$, i.e., the target velocity is 0 m/s, $F = 1$. From (30), it is easy to know that ISR $= 1$ and 1 is also the maximal value of ISR. When the target velocity is not 0 m/s, (30) can be derived as

$$\begin{aligned} \text{ISR} &= \left| \frac{F\left(1-F^{N_\text{s}-1}\right)}{(N_\text{s}-1)(1-F)} \right|^2 \\ &= \frac{1}{(N_\text{s}-1)^2} \left| \frac{F^{\frac{N_\text{s}+1}{2}} \left(F^{-\frac{N_\text{s}-1}{2}} - F^{\frac{N_\text{s}-1}{2}} \right)}{F^{\frac{1}{2}} \left(F^{-\frac{1}{2}} - F^{\frac{1}{2}} \right)} \right|^2 \\ &= \frac{1}{(N_\text{s}-1)^2} \left| \frac{F^{\frac{N_\text{s}}{2}} \left\{ -2j \sin\left[\pi (N_\text{s}-1) f_\text{D} T_\text{s}\right] \right\}}{2j \sin\left(\pi f_\text{D} T_\text{s}\right)} \right|^2 \\ &= \frac{1}{(N_\text{s}-1)^2} \left\{ \frac{\sin\left[\pi (N_\text{s}-1) f_\text{D} T_\text{s}\right]}{\sin\left(\pi f_\text{D} T_\text{s}\right)} \right\}^2 \\ &= \frac{1}{N_\text{s}-1} F_{N_\text{s}-1}\left(2\pi f_\text{D} T_\text{s}\right), \end{aligned} \tag{67}$$

where $N_\text{s} \geq 2$, $N_\text{s} \in \mathbb{Z}_{++}$, and the first equality in (67) using the sum of the geometric sequence. In addition, the third equality comes from the Euro's Formula.

The zero point of ISR occurs when the numerator of the Fejér kernel is zero while the denominator is non-zero. Thus, zero points occur when both $f_\text{D} T_\text{s} = k/(N_\text{s}-1),\ k = 1, 2, \ldots$ and $f_\text{D} T_\text{s} \neq k,\ k = 1, 2, \ldots$. For example, the first zero point occurs at $f_\text{D} T_\text{s} = 1/(N_\text{s}-1)$. Therefore, the minimal value of ISR is 0. However, since N_s is an integer while $1/(f_\text{D} T_\text{s})$ is a non-integer, it is impossible for ISR to be 0. In conclusion, the value range of ISR is (0,1].

Appendix C
Proof of (59)

Based on (16) and (58), the output signal after F-LS at a single subcarrier can be derived as

$$\begin{aligned} \bar{R}_{n,m}^{\text{F-LS}} &= H_{n,m} X_{n,m} + N_{n,m} \\ &\quad - X_{n,m} \frac{\sum_{s=0}^{N_\text{s}-1} \left(H_{n,s} |X_{n,s}|^2 + N_{n,s} X_{n,s}^* \right)}{\sum_{s=0}^{N_\text{s}-1} |X_{n,s}|^2} \\ &= \left(H_{n,m}^M + H_{n,m}^S \right) X_{n,m} \\ &\quad - X_{n,m} \frac{\sum_{s=0}^{N_\text{s}-1} \left(H_{n,s}^M + H_{n,s}^S \right) |X_{n,s}|^2}{\sum_{s=0}^{N_\text{s}-1} |X_{n,s}|^2} \\ &\quad + N_{n,m} - X_{n,m} \frac{\sum_{s=0}^{N_\text{s}-1} N_{n,s} X_{n,s}^*}{\sum_{s=0}^{N_\text{s}-1} |X_{n,s}|^2} \\ &= H_{n,m}^M X_{n,m} - \frac{X_{n,m}}{N_\text{s}} \sum_{s=0}^{N_\text{s}-1} H_{n,s}^M |X_{n,s}|^2 + N_{n,m} \\ &\quad - \frac{X_{n,m}}{N_\text{s}} \sum_{s=0}^{N_\text{s}-1} N_{n,s} X_{n,s}^*, \end{aligned} \tag{68}$$

where the last equation comes from $H^S_{n,m+1} = H^S_{n,m}$ and $\mathrm{E}[|X_{n,m}|^2] = 1$. Considering that the OFDM symbols are unitary modulus modulated, i.e., $|X_{n,s}|^2 = 1$, there is

$$\bar{R}^{\mathrm{F-LS}}_{n,m} = H^M_{n,m} X_{n,m} - \frac{X_{n,m}}{N_{\mathrm{s}}} \sum_{s=0}^{N_{\mathrm{s}}-1} H^M_{n,s} + N_{n,m} - \frac{X_{n,m}}{N_{\mathrm{s}}} \sum_{s=0}^{N_{\mathrm{s}}-1} \frac{N_{n,s}}{X_{n,s}}. \tag{69}$$

REFERENCES

[1] J. A. Zhang et al., "Enabling joint communication and radar sensing in mobile networks–A survey," *IEEE Commun. Surveys Tuts.*, vol. 24, no. 1, pp. 306–345, First Quarter 2022.

[2] F. Liu et al., "Integrated sensing and communications: Toward dual-functional wireless networks for 6G and beyond," *IEEE J. Sel. Areas Commun.*, vol. 40, no. 6, pp. 1728–1767, Jun. 2022.

[3] W. Xu, Z. Yang, D. W. K. Ng, M. Levorato, Y. C. Eldar, and M. Debbah, "Edge learning for B5G networks with distributed signal processing: Semantic communication, edge computing, and wireless sensing," *IEEE J. Sel. Topics Signal Process.*, vol. 17, no. 1, pp. 9–39, Jan. 2023.

[4] C. Sturm and W. Wiesbeck, "Waveform design and signal processing aspects for fusion of wireless communications and radar sensing," *Proc. IEEE*, vol. 99, no. 7, pp. 1236–1259, Jul. 2011.

[5] C. B. Barneto et al., "Full-duplex OFDM radar with LTE and 5G NR waveforms: Challenges, solutions, and measurements," *IEEE Trans. Microw. Theory Techn.*, vol. 67, no. 10, pp. 4042–4054, Oct. 2019.

[6] C. B. Barneto, S. D. Liyanaarachchi, M. Heino, T. Riihonen, and M. Valkama, "Full duplex radio/radar technology: The enabler for advanced joint communication and sensing," *IEEE Wireless Commun*, vol. 28, no. 1, pp. 82–88, Feb. 2021.

[7] M. F. Keskin, H. Wymeersch, and V. Koivunen, "MIMO-OFDM joint radar-communications: Is ICI friend or foe?," *IEEE J. Sel. Topics Signal Process.*, vol. 15, no. 6, pp. 1393–1408, Nov. 2021.

[8] Y. Huang, S. Hu, S. Ma, Z. Liu, and M. Xiao, "Designing low-PAPR waveform for OFDM-based RadCom systems," *IEEE Trans. Wirel. Commun.*, vol. 21, no. 9, pp. 6979–6993, Sep. 2022.

[9] M. Malanowski, *Signal Processing for Passive Bistatic Radar*. Norwood, MA, USA: Artech House, 2019.

[10] C. G. Tsinos, A. Arora, S. Chatzinotas, and B. Ottersten, "Joint transmit waveform and receive filter design for dual-function radar-communication systems," *IEEE J. Sel. Topics Signal Process.*, vol. 15, no. 6, pp. 1378–1392, Nov. 2021.

[11] C. B. Barneto, T. Riihonen, S. D. Liyanaarachchi, M. Heino, N. González-Prelcic, and M. Valkama, "Beamformer design and optimization for joint communication and full-duplex sensing at mm-Waves," *IEEE Trans. Commun.*, vol. 70, no. 12, pp. 8298–8312, Dec. 2022.

[12] Z. He, W. Xu, H. Shen, D. W. K. Ng, Y. C. Eldar, and X. You, "Full-duplex communication for ISAC: Joint beamforming and power optimization," *IEEE J. Sel. Areas Commun.*, vol. 41, no. 9, pp. 2920–2936, Sep. 2023.

[13] Z. Liu, S. Aditya, H. Li, and B. Clerckx, "Joint transmit and receive beamforming design in full-duplex integrated sensing and communications," *IEEE J. Sel. Areas Commun.*, vol. 41, no. 9, pp. 2907–2919, Sep. 2023.

[14] K. E. Kolodziej, B. T. Perry, and J. S. Herd, "In-band full-duplex technology: Techniques and systems survey," *IEEE Trans. Microw. Theory Tech.*, vol. 67, no. 7, pp. 3025–3041, Jul. 2019.

[15] D. Korpi, M. Heino, C. Icheln, K. Haneda, and M. Valkama, "Compact inband full-duplex relays with beyond 100 dB self-interference suppression: Enabling techniques and field measurements," *IEEE Trans. Antennas Propag.*, vol. 65, no. 2, pp. 960–965, Feb. 2017.

[16] J. P. Doane, K. E. Kolodziej, and B. T. Perry, "Simultaneous transmit and receive with digital phased arrays," in *Proc. IEEE Int. Symp. Phased Array Syst. Technol.*, 2016, pp. 1–6.

[17] K. E. Kolodziej, B. A. Janice, A. I. Sands, and B. T. Perry, "Scalable in-band full-duplex phased arrays: Complexity reduction and distributed processing," *IEEE J. Sel. Areas Commun.*, vol. 41, no. 9, pp. 2808–2820, Sep. 2023.

[18] C. Shi, W. Pan, Y. Shen, and S. Shao, "Robust transmit beamforming for self-interference cancellation in star phased array systems," *IEEE Signal Process. Lett.*, vol. 29, pp. 2622–2626, 2022.

[19] M. Adams and V. K. Bhargava, "Use of the recursive least squares filter for self interference channel estimation," in *Proc. IEEE Veh. Technol. Conf.*, 2016, pp. 1–4.

[20] M. S. Amjad and O. Gurbuz, "Linear digital cancellation with reduced computational complexity for full-duplex radios," in *Proc. IEEE Wirel. Commun. Netw. Conf.*, 2017, pp. 1–6.

[21] K. Komatsu, Y. Miyaji, and H. Uehara, "Basis function selection of frequency-domain Hammerstein self-interference canceller for in-band full-duplex wireless communications," *IEEE Trans. Wireless Commun.*, vol. 17, no. 6, pp. 3768–3780, Jun. 2018.

[22] Y. He, H. Zhao, W. Guo, S. Shao, and Y. Tang, "Frequency-domain successive cancellation of nonlinear self-interference with reduced complexity for full-duplex radios," *IEEE Trans. Commun.*, vol. 70, no. 4, pp. 2678–2690, Apr. 2022.

[23] F. Colone, D. W. O'Hagan, P. Lombardo, and C. J. Baker, "A multistage processing algorithm for disturbance removal and target detection in passive bistatic radar," *IEEE Trans. Aerosp. Electron. Syst.*, vol. 45, no. 2, pp. 698–722, Apr. 2009.

[24] S. Zhang, S.-C. Liew, and H. Wang, "Blind known interference cancellation," *IEEE J. Sel. Areas Commun.*, vol. 31, no. 8, pp. 1572–1582, Aug. 2013.

[25] D. Liu, B. Zhao, F. Wu, S. Shao, X. Pu, and Y. Tang, "Semi-blind SI cancellation for in-band full-duplex wireless communications," *IEEE Commun. Lett.*, vol. 22, no. 5, pp. 1078–1081, May 2018.

[26] X. Quan, Y. Liu, D. Chen, S. Shao, Y. Tang, and K. Kang, "Blind nonlinear self-interference cancellation for wireless full-duplex transceivers," *IEEE Access*, vol. 6, pp. 37725–37737, 2018.

[27] J. G. Proakis and M. Salehi, *Digital Communications*, 5th ed. New York, NY, USA: McGraw-Hill, 2008.

[28] G. Hakobyan and B. Yang, "A novel intercarrier-interference free signal processing scheme for OFDM radar," *IEEE Trans. Veh. Technol.*, vol. 67, no. 6, pp. 5158–5167, Jun. 2018.

[29] E. M. Stein and R. Shakarchi, *Fourier Analysis: An Introduction*. Princeton, NJ, USA: Princeton Univ. Press, 2003.

[30] M. Braun, "OFDM radar algorithms in mobile communication networks," Ph.D. dissertation, Karlsruher Institut of Technologie, Karlsruhe, Germany, Jan. 2014.

[31] M. A. Richards, *Fundamentals of Radar Signal Processing*, 2nd ed. New York, NY, USA: McGraw-Hill, 2014.

[32] U. Meyer-Baese, *Digital Signal Processing With Field Programmable Gate Arrays*, 4th ed. Berlin, Germany: Springer, 2014.

[33] S. Haykin, *Adaptive Filter Theory*, 5th ed. London, U.K.: Pearson, 2013.

[34] E. Marchetti, L. Daniel, E. G. Hoare, F. Norouzian, M. Cherniakov, and M. Gashinova, "Radar reflectivity of a passenger car at 300 GHz," in *Proc. 19th Int. Radar Symp.*, 2018, pp. 1–7.

Baiyu Duan (Student Member, IEEE) was born in Sichuan, China, in 1996. He received the B.E. degree in electronic and information engineering in 2019 from the University of Electronic Science and Technology of China (UESTC), Chengdu, China, where he is currently working toward the Ph.D. degree in information and communication engineering with the National Key Laboratory of Wireless Communications. His research interests include interference cancellation, full-duplex communications, and integrated sensing and communications.

Cong Chen was born in Henan, China, in 1990. He received the B.E. degree in communication engineering and the M.S. degree in electronic and communication engineering in 2012 and 2015, respectively, from the University of Electronic Science and Technology of China, Chengdu, China, where he is currently working toward the Ph.D. degree in electronics and information with the National Key Laboratory of Wireless Communications. His research interests include interference cancellation, time synchronization, and ad hoc networks.

Wensheng Pan was born in Chongqing, China, in 1975. He received the B.E., M.S, and Ph.D. degrees in communication engineering from the University of Electronic Science and Technology of China (UESTC), Chengdu, China, in 1998, 2005, and 2015, respectively. He is currently an Assistant Researcher with the National Key Laboratory of Wireless Communications, UESTC. His research interests include power amplifier design, power amplifier linearization, digital predistortion, and crest factor reduction.

Ying Shen was born in Sichuan, China, in 1978. He received the B.E., M.S., and Ph.D. degrees in communication engineering from the University of Electronic Science and Technology of China (UESTC), Chengdu, China, in 2003, 2006, and 2009, respectively. He is currently a Researcher with the National Key Laboratory of Wireless Communications, UESTC. His research interests include antijamming technologies, full-duplex communications, and signal processing in wireless communications.

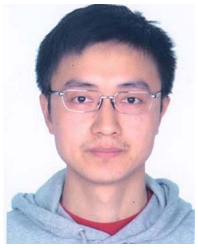

Ying Liu (Senior Member, IEEE) received the B.E. and M.S. degrees in communication engineering and the Ph.D. degree in communication and information systems from the University of Electronic Science and Technology of China (UESTC), Chengdu, China, in 2008, 2011, and 2016, respectively. He is currently an Assistant Professor with the National Key Laboratory of Wireless Communications, UESTC. He was a Visiting Scholar with the Department of Electrical and Computer Engineering, Ohio State University, Columbus, OH, USA. His research interests include wireless communication system design, nonlinear modeling, digital predistortion, full duplex communications, and signal processing in wireless communications.

Shihai Shao (Member, IEEE) was born in Liaoning, China, in 1980. He received the B.E. and Ph.D. degrees in communication and information systems from the University of Electronic Science and Technology of China (UESTC), Chengdu, China, in 2003 and 2008, respectively. He is currently with the National Key Laboratory of Wireless Communications, UESTC, as a Professor. His research interests include wireless communications, spread spectrum, and distributed multiple-input multiple-output detection.